Fall 2016

Development of high-performance cast steel crankshafts

Lucas Andrew Archer
University of Iowa

DEVELOPMENT OF HIGH-PERFORMANCE CAST STEEL CRANKSHAFTS

by

Lucas Andrew Archer

A thesis submitted in partial fulfillment
of the requirements for the Master of Science
degree in Mechanical Engineering in the
Graduate College of
The University of Iowa

December 2016

Thesis Supervisor: Professor Christoph Beckermann

Graduate College
The University of Iowa
Iowa City, Iowa

CERTIFICATE OF APPROVAL

MASTER'S THESIS

This is to certify that the Master's thesis of

Lucas Andrew Archer

has been approved by the Examining Committee for
the thesis requirement for the Master of Science degree
in Mechanical Engineering at the December 2016 graduation.

Thesis Committee: _____
Christoph Beckermann, Thesis Supervisor

_____
H. S. Udaykumar

_____
Albert Ratner

ACKNOWLEDGEMENTS

I would like to thank my advisor, Professor Christoph Beckermann, for the opportunity to accomplish this work, for his abundance of advice, and continued direction throughout this project. I want to express my gratitude to my thesis committee, Professors Albert Ratner and H.S. Udaykumar for lending me their valuable time. I want to thank all of the members of the Solidification Laboratory for their support, especially Richard Hardin, for the experimental and computational teachings. I also want to thank Jerry Thiel, Sairam Ravi, and all the staff and students at the University of Northern Iowa Metal Casting Center for their assistance with the casting experiments. Finally, I would like to thank my parents for their love and support, and my sister for proof reading my thesis.

ABSTRACT

To produce cast steel crankshafts, risering and gating systems are developed. Filling and solidification simulations of the steel crankshaft rigging are carried out to confirm that the rigging developed will produce a low porosity casting. A sand mold is created with Computer-aided design software, based on the developed crankshaft and rigging. Two prototype crankshafts are cast from the sand molds, and analyzed for porosity. The porosity analysis results are compared directly to the simulated porosity, and found to be in good agreement. From the analysis of the prototype crankshaft, rigging systems for a two-on and single-throw crankshaft are developed.

A new casting method for steel is developed. The counter-gravity with pressurization during solidification casting method utilizes vacuum pressure of 7.3 psia to draw liquid steel into a mold, where it is held until the inlet has solidified. Once the inlet has solidified, the vacuum pressure is released, and the pressure of the entire system is raised to 45 psia. Exothermic hot topping keeps the top of the riser liquid while the rest of the casting forms a solid shell. Therefore, the pressure only acts on the liquid metal at the top of the riser, forcing the liquid metal to feed farther into the casting. The new method is tested with simple bar castings. Analysis of cast bars shows that centerline porosity is fed by the riser when pressurized, while the gravity-filled control casting is not.

PUBLIC ABSTRACT

Crankshafts of the modern engine are either cast iron or forged steel. As the automotive industry continues to move towards higher-performance and more efficient engines, the weaker cast iron crankshaft will no longer meet the durability requirements needed for high-performance engines. On the other hand, forged steel crankshafts meet these requirements, however they are costly to produce and the nature of their production does not allow for hollow sections, which improve fuel efficiency. A cast steel crankshaft combines the benefits of both cast iron and forged steel crankshafts. Steel castings are cheaper than forging and can be made to meet the mechanical properties of forgings with good casting techniques and processes.

Counter-gravity filling and applying pressure while the casting is solidifying are both beneficial casting processes. Counter-gravity filling allows the liquid steel to be pulled gently into a mold, as opposed to dumping the metal down a sprue. Steel shrinks when it solidifies, therefore it is necessary to add extra reservoirs of steel above the mold cavity, called risers. Traditionally the weight of the riser presses the liquid metal down into the casting to compensate for the shrinking steel. This effect is limited, so applying extra pressure to the top of the riser increases the effectiveness of the riser and can reduce the defects caused by the shrinking steel. In a newly developed method, vacuum pressure is used to draw molten steel smoothly into a mold and after the mold inlet has solidified the casting is pressurized, which forces the liquid steel in the riser down into the casting.

TABLE OF CONTENTS

LIST OF TABLES

Table

LIST OF FIGURES

Figure

LIST OF NOMENCLATURE

Acronyms

CFPS	Counter-gravity Filling with Pressurization during Solidification
CAD	Computer-aided Design
LSVAC	Loose Sand Vacuum Assisted Casting process
APC	Adjusted Pressure Casting
GM	General Motors Company
SGE	Small Gas Engine
UNIMCC	University of Northern Iowa's Metal Casting Center
EMT	Element Materials Technology

CHAPTER 1: INTRODUCTION

1.1 Motivation

1.1.1 High-performance Cast Steel Crankshafts

The current methods of manufacturing crankshafts include casting with iron or forging in steel. Cast iron crankshafts are a relatively low cost for high production [1], while forged steel crankshafts offer a greater fatigue life in high-performance engines [2]. Due to the increasing need for high-performance, high-efficiency engines in both the automotive and industrial vehicles, cast iron crankshafts may not continue to meet the strength and fatigue criteria. At the same time, forged steel crankshafts, are able to meet strength and fatigue criteria, but are not as cheaply manufactured as cast crankshafts. The forging manufacturing process also limits the ability to reduce the weight of the crankshaft by hollowing out journals, which is easily done in metal casting. Reducing the weight of the crankshaft improves the fuel efficiency of the engine.

A high-performance cast steel crankshaft combines the benefits of both aforementioned crankshaft-manufacturing processes. Steel is a stronger metal than iron, and the casting process allows for the use of cores to create hollow sections, which leads to a lighter more efficient crankshaft. Currently, cast steel crankshafts are not manufactured on a large scale. In order to mass-produce cast steel crankshafts, it is first necessary to design a gating and riser system. A gating system includes the sprue, runner, and gates, which bring the liquid steel into the mold cavity. Risers are extra reservoirs of liquid metal used to feed the casting as the steel shrinks during solidification. Second, clean steel casting methods can be developed to ensure consistent quality of the crankshafts during production. The benefits outlined are the reason a collaborative research project, sponsored by the Department of Energy, General Motors and Caterpillar, formed to

develop cast steel alloys and processing techniques that allow cast steel crankshafts to achieve target properties of forged crankshafts.

1.1.2 Counter-gravity Filling

Traditionally steel castings are produced by pouring molten steel into a mold, which is called gravity filling. Liquid metal flows down a sprue, until it reaches the bottom of a runner. The metal flows through the runner until it reaches the gate where the metal enters the cavity of the cast part. Air can become entrained within the melt as the liquid metal falls and splashes down at the bottom of the sprue and waterfalls down valleys within the mold cavity. When air is entrained within the casting, reoxidation inclusions form as the deoxidized steel is exposed to oxygen [3]. One solution to dramatically reducing air entrainment is counter-gravity casting [4].

Counter-gravity casting is a method of casting in which liquid metal is pushed using positive pressure, or pulled using vacuum pressure into a mold cavity. With this casting method, it is possible to eliminate splashing and waterfalls present in traditional gravity poured castings. By controlling the filling pressure, the liquid metal's critical velocity [5] can be avoided, filling the mold smoothly and quiescently. Counter-gravity filling with vacuum pressure can be readily implemented in existing foundry systems, without any modification to the furnace. The sand mold is placed within an airtight chamber, which is then placed directly above the furnace. Using vacuum pressure the liquid steel is drawn into the mold, and when the inlet to the casting has solidified, the chamber can be removed from the furnace.

1.1.3 Pressurization During Solidification

Steel contracts during solidification. Therefore, it is necessary to provide the casting with extra liquid metal, called risers, to feed the shrinkage cause by solidification. Risers are generally used in all steel castings. Risers along with the gating systems are removed from the casting during

post-processing, and are considered waste. One measure of efficiency for a casting is the casting yield, which is the weight ratio between all metal used for the casting and the cast part. Reducing the size and number of risers on a casting increases the casting yield. However, risers have an optimum size and spacing necessary to prevent shrinkage defects [6].

One method to increase the effectiveness of risers is to apply pressure to the risers. The application of increased (above atmospheric) pressure on risers during solidification has been shown to assist the feeding of metal castings, which in turn reduces the level of porosity in the casting and allows for the use of smaller risers [7]. While previous studies have pressurized only the riser of the castings, it is possible to subject the entire casting to an increase in pressure and retain the same benefits. Provided the top of the riser remains liquid and the exterior of the casting has solidified into a sufficiently thick shell, only the top of the riser will be effected by the increased pressure. This method of riser pressurization pairs well with counter-gravity filling, as the casting already resides within an airtight vessel.

1.2 Objective of the Present Study

The objective of this work is two-fold. First, a rigging and riser system will be designed, simulated, and tested for a cast steel crankshaft. The rigging and riser system will be designed with the goal of minimizing porosity while keeping post-casting processing costs low. Second, an investigation of the effects of Counter-gravity filling with pressurization during solidification (CFPS) on steel casting will be performed to determine if this casting method offers benefits towards manufacturing high-performance cast steel crankshafts.

In the present study, a gating and riser system is developed in an iterative fashion using computer-aided design (CAD) modeling software in conjunction with the metal casting simulation software *MAGMAsoft* [8] to create a traditional gravity-filled cast steel crankshaft mold. Two

crankshaft sand molds are 3D printed and cast in a low-alloy steel. The castings are analyzed for porosity, with radiography, dye-penetrant, and microphotography. The analysis results are compared directly to the *MAGMAsoft* porosity predictions, to determine what modifications can be made to improve the gating and riser system. A two-on crankshaft gating system is designed for future casting of cast steel crankshafts.

A CFPS system is designed and tested, using a cylindrical bar casting. This casting shape is chosen because centerline shrink, or porosity, occurs naturally without the use of pressurization during solidification. The filling of the casting is simulated using *MAGMAsoft* to ensure that the mold filled quiescently. For the CFPS experiment, vacuum pressure is used to fill the molds and when the mold inlet has solidified, the entire vessel containing the mold is pressurized. Two gravity-filled castings are designed and cast to serve as control cases for the CFPS castings, these castings also use the same cylindrical bar casting with the addition of a runner and sprue for filling. Radiographs and dye-penetrant tests are taken with the gravity-filled and CFPS castings to compare the porosity between the two castings.

The size of the crankshaft examined is incompatible with the designed CFPS system so a single-throw of the crankshaft is used to test the CFPS system. A single-throw crankshaft is a partial section of a full crankshaft that can be subjected to high-cycle fatigue testing in the same manner as a full crankshaft. A rigging and riser system is developed for the single-throw crankshaft, so the effects of CFPS can be examined on a more complex casting. The filling of the single-throw crankshaft is simulated with *MAGMAsoft*, to ensure that the porosity predicted will be analogous to the porosity found in the full-sized crankshaft.

CHAPTER 2: LITERATUTRE REVIEW

2.1 Introduction

Cast iron and forged steel crankshafts for automotive and industrial vehicles have been produced by countless companies for the past century. For the most part, cast steel crankshafts have been neglected in both industries. Literature regarding production of cast steel crankshaft is sparse. Literature covering counter-gravity casting or pressurization during solidification for steel alloys is readily accessible; however, research regarding the combination of these two processes is limited to other metals such as aluminum and nickel alloys. This chapter will review; 1) briefly, previous cast steel crankshafts production in the automotive industry; 2) previous counter-gravity casting methods for steel and experiments; 3) previous experiments of pressurization during solidification of steel, and an examination of adjusted pressure casting technique with nickel-alloy, which is a combination of counter-gravity filling and pressurization during solidification.

2.2 Production of Cast Steel Crankshafts

In the present day, cast steel crankshafts for automotive and industrial vehicles are not produced on large-scale. In 1935, Sorensen filed for a patent for a mold pattern, shown in Figure 2.1, for the production of cast steel crankshafts for Ford Motor Company's Flathead V8 engine [9]. Sorensen's mold cast four crankshafts simultaneously, and utilized a large central sprue to feed most of the casting. It is unclear from the literature when the production of these cast steel crankshafts ceased, but today's crankshafts are manufactured predominantly, with either cast iron or forged steel.

2.3 Counter-gravity Casting Steel

For the past thirty years, counter-gravity casting of steel has been a proven method to reliably obtain quality parts. In 1982, Chandley et al. [10] patented a counter-gravity steel casting process. In this process a gas permeable mold was placed within a chamber. The mold's lower surface was placed directly on top of the liquid metal reservoir, with the gates to the casting cavity submerged. A vacuum pressure was applied to the top of the mold, which filled the mold cavities with molten steel. In this method, multiple disconnected parts were cast without the extra metal of the runner. One disadvantage of this process was the bonded sand in contact with the melt reservoir failed after 5 to 20 seconds for high-temperature melting alloys such as steel. The maximum vacuum pressure was limited to -1.0 to -3.0 psig in order to prevent penetration of the gas permeable mold by the liquid metal. This in turn limited the maximum height of the castings that could be cast to 6 to 8 inches.

Chandley et al. [11] further refined their counter-gravity casting process, with the introduction of the loose sand vacuum assisted casting process (LSVAC), shown in Figure 2.2. A thin-shelled investment mold was used rather than a large bonded sand mold. The molds were then backed with cheaper loose sand, hence the name. The thinner molds allowed for more castings per process cycle, as well as more freedom in mold orientation within the chamber. The LSVAC process excelled at creating thin-walled stainless steel castings, such as an automotive exhaust manifold. Chandley et al. compared three exhaust manifolds created by different manufacturing processes with a thermal fatigue test. A manifold fabricated from 409 stainless steel, a cast high silicon-molybdenum nodular cast iron manifold, and a cast stainless steel manifold created with the LSVAC process, were all tested. The test involved cycling the manifolds through the temperatures between 20° C and 900 °C. Both the cast iron exhaust manifold and the fabricated

stainless steel manifold developed cracks after 600 cycles, while the LSVAC stainless steel manifold lasted more than 1800 cycles. It was noted that the cast stainless steel manifold had a thicker wall than the fabricated, so it may not have experienced as extreme of thermal cycling. However, Chandley et al. pointed to economic data stating, that the fabricated manifold was created with 14 different parts, needing 15 welds, which lead to a higher cost part than the manifold created with the LSVAC process.

Griffiths et al. [12] investigated the effects that four different casting methods had on the reproducibility of the mechanical properties for low alloy steel investment castings. Plate castings (105 mm x 25 mm x 10 mm) were cast and tensile test bars were cut from the plates. Two different gravity poured refractory molds were used. One mold was filled so that the liquid steel was poured directly into the part cavity. The second gravity-poured casting included a more conventional gating system, with a runner that delivered the metal from below the part cavity. Two counter-gravity processes were used in addition to the gravity poured molds. The first is the so-called Hitchiner design, in which metal is drawn up a large central sprue with vacuum pressure and multiple parts are filled. When the gates to the parts have solidified, the vacuum pressure is released and the metal remaining within the sprue falls back into the furnace below. The second counter-gravity process tested was the C^3 method. Developed by Hitchiner Manufacturing Co., Inc., the investment mold is filled in the same way as the Hitchiner design, but during solidification centrifugal force is used to assist the feeding of the parts. When the centrifuge process is complete the metal remaining in the sprue is returned to the furnace.

The tensile bars were tested to obtain the ultimate tensile strength and percent elongation values. These two mechanical properties were used to create Weibull modulus plot. The Weibull modulus was used to describe the variance of mechanical properties from a process, with the larger

modulus representing a more reliable casting process. After calculating the Weibull modulus for each casting process, Griffiths et al. found that both counter-gravity methods produced castings more reliably than either of the gravity-poured. The C^3 process had the greatest Weibull modulus. It was speculated that the higher Weibull moduli of the counter-gravity processes occurred due to the decrease in splashing and turbulence during filling, and the cleaner steel accessed by the counter-gravity process in the lower half of the furnace.

2.4 Pressurization During Solidification

Pressurization during solidification of metals assists feeding and reduces porosity in castings. Jazwinski and Finch [13] in 1945, used gas producing cartridges in blind risers as a source of pressure. The cartridges were in the risers before filling and released their pressure after an adequate shell had formed on the riser, so that the increase in pressure was applied to the liquid at the top of the riser. Jazwinski and Finch found that pressuring the risers would increase the casting yield because smaller pressurized risers would feed as far as larger non-pressurized risers.

Rather than gas cartridges, Taylor [14] utilized a pipe extending from the riser and nitrogen gas to pressurize the riser. Again, after a significant shell had formed the riser was pressurized. Taylor's method allowed for more control of the magnitude of the pressure, length of time the risers were pressurized, and control the variable pressure over time. A variety of casting shapes were tested and Taylor showed that occasionally the pressurized riser produced sound castings, where non-pressurized risers would not. However, he was not able to reproduce the effect easily. It was concluded that, pressures from 3 to 50 psig were more beneficial than higher pressures in the few successful cases. The rate and timing of the pressurization was critical to prevent enlarging the casting, metal mold penetration, and forcing metal back out of the sprue. Temperature gradients within the steel were still the largest determining factor when making sound castings.

One critique of Taylor's experiment was that he was attempting the technique on relatively small castings. Desnizki [15], chose to test pressurization on a variety of large castings. By using a vent with compressed air to pressurize the riser from both the top and within, Desnizki, improved the sealing of the riser with a grey iron cover over the riser. An exothermic sleeve was used to keep the riser liquid longer, which improved the feeding of the casting. With this method, pressure was raised 0.2 atm. above gauge after 4 minutes, then by 0.2 atm. every 2 minutes until a final pressure of 5.0 atm. above gauge was reached and held for the remaining 1.5 hours of the experiment. When the mold was opened the riser had completely vanished. Despite this, the pressurization allowed the sections of a long bar casting furthest away from the riser to be porosity-free. Casting yields were dramatically increased, upwards of 82.5% for steel and iron castings. It was noted that effect of the pressure was not enough to guarantee porosity free sections in cast parts and thickened sections.

More recently, Harden et al. [7] performed a series of trials, which compared 3" thick by 6" wide steel plate castings produced with and without pressurizing the risers. In the first trial, 31.5" long plates with a 6" diameter by 8" riser at one end, were used. A ceramic riser cap was used to contain the pressure, and argon gas was fed through a fusil tube as the pressurizing gas. For the second trial, the plate length was increased to 39" and the riser cap was removed, and instead a seal between the steel shell and fusil tube was utilized. The third trial further extended the length of the plate to 50", and the casting was filled from the opposite end of the riser, unlike the first two trials where the casting was filled from the riser. A variety of pressure schedules were used in each trial. Radiographs of the first trial's castings yielded virtually no difference between the pressurized plates and non-pressurized plates, the risers of the non-pressurized case fed the castings more than anticipated, hence the increase in length for the remaining trials. In the second

trial, the pressurized plate was far sounder in radiographs than the non-pressurized castings showing that pressurization can increase the feeding length of a riser. The third trial confirmed the findings of the second trial. Pressurization of the riser increased the feeding length of the riser by a factor of nearly five. The experiment concluded that centerline shrinkage porosity could be eliminated by pressurizing the riser. A time delay of the pressurization is necessary, because a minimum surface solid fraction of 0.7 was found to be optimum in order to prevent mold penetration. A pressure range between 15 and 28 psig was used successfully to improve the soundness of the castings.

Counter-gravity adjusted pressure casting (APC) is a process that combines the benefits of both counter-gravity filling and pressurization during solidification. APC is predominantly used in casting large, thin walled nonferrous alloy castings. Dong et al. [16] investigated IN718, a nickel based alloy cast using the APC process. The diagram of the APC equipment is shown in Figure 2.3. The APC process proceeds as follows. First, a ceramic shell mold and rising tube are placed inside the upper chamber. The rising tube is inserted into molten alloy. Next, the liquid metal is drawn up the rising tube with vacuum pressure into the mold within the upper chamber. The vacuum pressure is held until the inlet to the mold has solidified. Finally, the entire upper chamber is pressurized at a rate of 3kPa/s, and held. An example of the pressure throughout the process is shown in Figure 2.4. Three thin plates were cast with the APC process, with varied holding pressure for each plate casting. Dong et al. observed that the average grain size decreased with increased holding pressure, they proposed that the force of the pressure drove the metal flow and broke dendrites while their strength was low. This resulted in an increase of crystal nucleus and grain refinement.

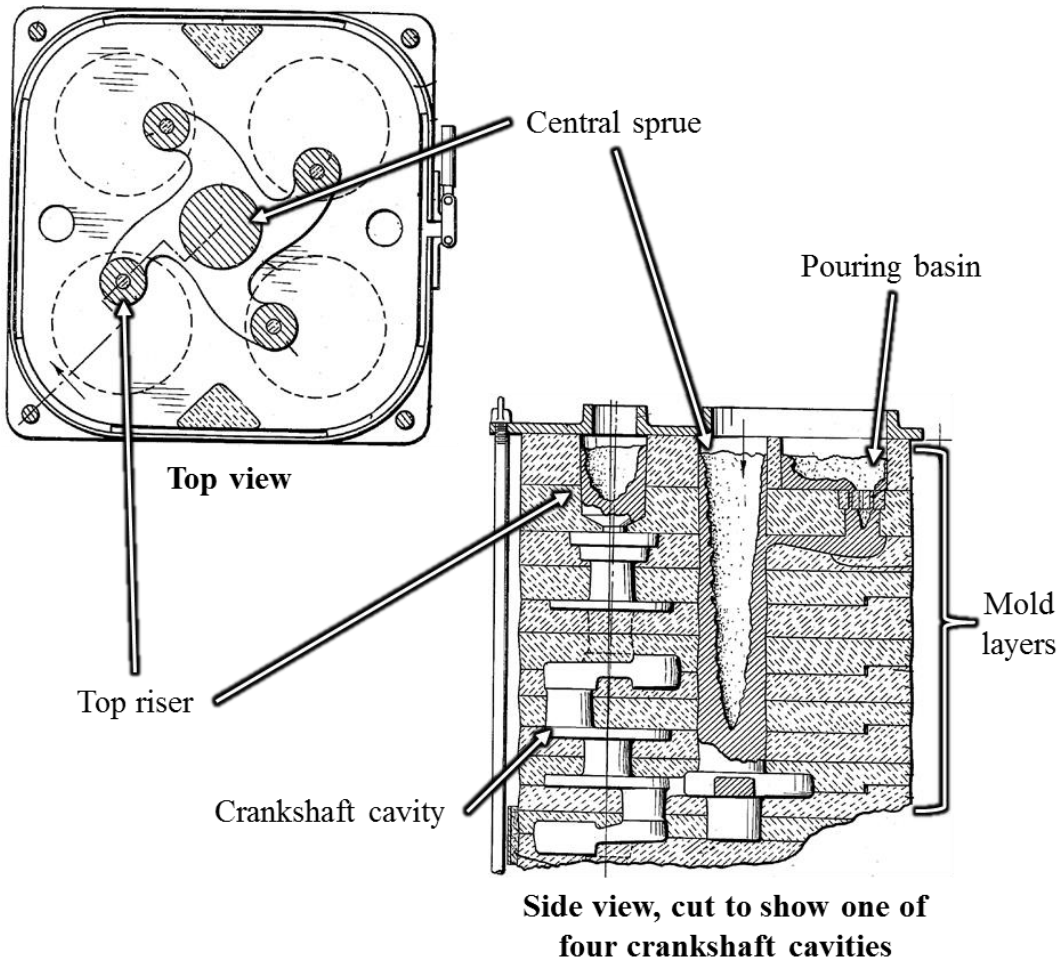

Figure 2.1 Diagram of mold pattern for Ford Motor Company's Flat Head V8 steel crankshaft. Adapted from [9].

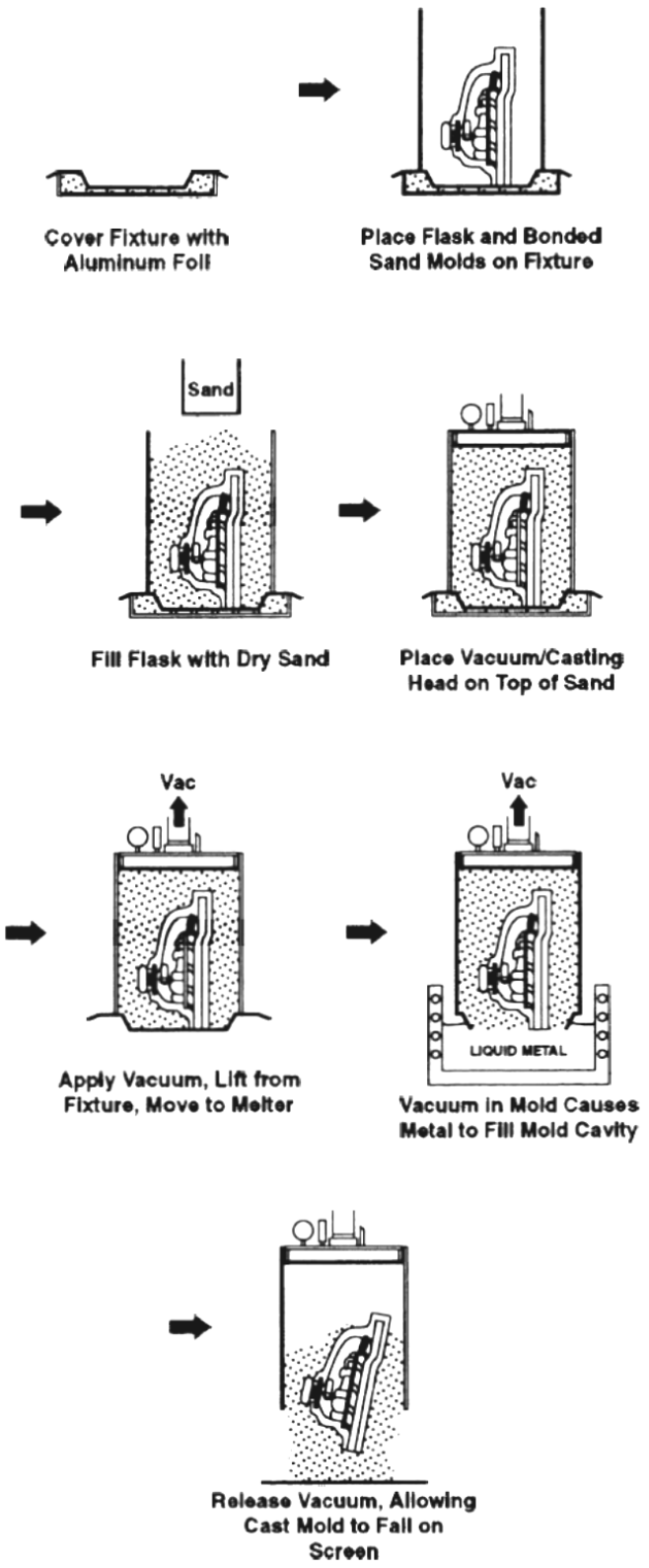

Figure 2.2 LSVAC process invented by Chandley et al. Adapted from [11].

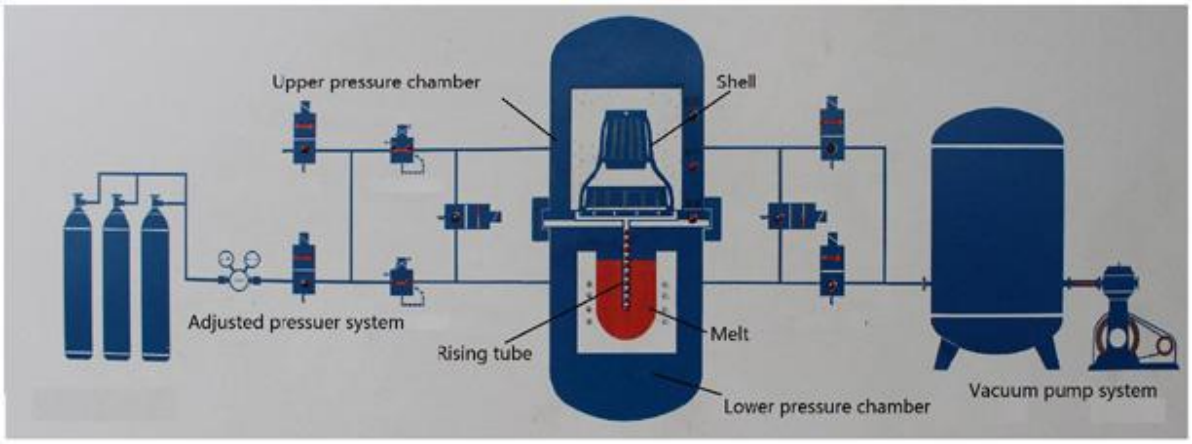

Figure 2.3 Diagram of APC equipment. Adapted from [16].

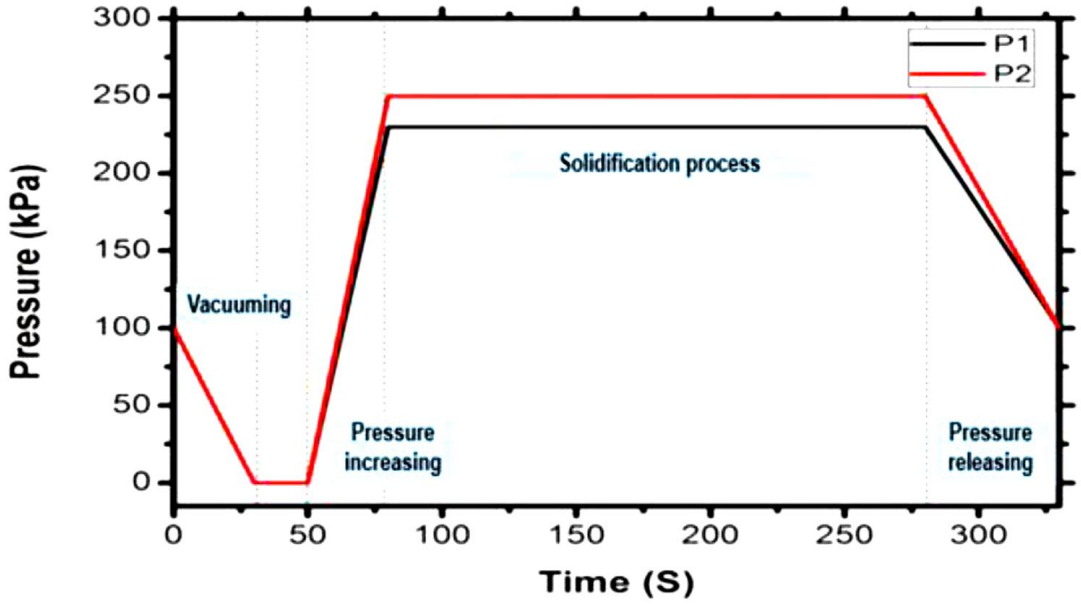

Figure 2.4 Pressure change in the upper (P1) and lower (P2) chamber during the APC process. Adapted from [16].

CHAPTER 3: DEVELOPMENT OF CAST STEEL CRANKSHAFT RIGGING

3.1 Introduction

While cast steel crankshafts were produced in the past, they have been replaced by forged steel crankshafts. This occurred due in part to the increase in performance of engines. The cast steel crankshafts of the past likely possessed high-levels of porosity caused by ineffective risering. This would lead to a decrease in high cycle fatigue life of the part, especially in high-performance engines. In the present day, it is possible to simulate filling and solidification of a casting. Therefore, it is necessary to first develop riser and gating systems utilizing computer aided design modeling and casting simulation software to ensure a defect free casting.

3.2 Crankshaft Rigging Design and Simulation

The rigging was designed for a General Motors Company (GM) small gas engine (SGE) crankshaft, shown in Figure 3.1. While other crankshafts were simulated, a vast majority of the rigging designed was for the GM SGE crankshaft. However, the concepts applied to this crankshaft could be applied to most other automotive or industrial vehicle crankshafts, because most crankshaft have similar geometries. The GM SGE crankshaft featured cored journals. All simulations were performed using *MAGMAsoft*, and Caterpillar's 1E1667mod low alloy steel was used as the simulated steel for the design process. The main focus when designing the rigging for the GM SGE crankshaft was to simulate a crankshaft with very low levels of porosity.

The first step to designing the rigging was to simulate the crankshaft, in a horizontal orientation without gating and risers, which is termed natural solidification. The porosity results from the natural solidification simulation, shown in Figure 3.2, were used to determine the initial placement of risers and a gating system for the crankshaft. In the natural solidification case large

amounts of porosity was located in the front and rear main journals as well in the webs adjacent to center connecting rod journals. The locations of high porosity are attributed to hot spots within the casting that needed to be fed with risers.

A riser placed in front of the rear main journal, shown in Figure 3.3, was found to be the most effective location to feed the crankshaft and removed most of the porosity near that location, Figure 3.4. The next step was to design a gating system for the crankshaft. The gating design was optimized to achieve a smooth flow with a total filling time of 10 seconds and an initial pouring temperature of 1600° C. A small porosity spot was located inside the rear main journal. A new core was added to the center of the rear main journal, shown in Figure 3.5, to prevent porosity at that location. The new core effectively removed porosity in that location, Figure 3.6, without causing new porosity to form elsewhere in the crankshaft.

One riser was not enough to ensure a sound casting so several additional risers were placed above locations that required additional feeding. The final risering is shown in Figure 3.7, two risers were added above the center connecting rod journals and to the center counter-weights. A riser was placed over the front main journal. Several iterations were simulated for each addition riser in order to obtain an optimum riser size while also minimizing the risers contact with the crankshaft. The four risers near the center of the crankshaft created a hot spot in the center main journal, so a chill was placed around this journal to separate the feeding of the four journals. Filling was simulated with a pouring time of 15 seconds and an initial pouring temperature of 1600° C. It is shown in Figure 3.8 that the simulation predicts very low porosity.

It was decided that the aforementioned design would be a suitable choice for the first round of crankshafts to be cast at a foundry. The sand mold of the casting would be created using the 3D printer at the University of Northern Iowa's Metal Casting Center (UNIMCC). In order to print

the mold a 3D model of the mold was required. To create the 3D model of the sand mold, the CAD software, *Creo Parametric 2.0* was used to rebuild the rigging originally created in *MAGMAsoft*. The mold was divided into a cope and drag, Figure 3.9 and Figure 3.10, respectively.

Vents were added to the mold. Some vents lead directly to the crankshaft cavity, others resided only in the sand of the mold to prevent binder gas from becoming entrapped near the casting surface. The height of the vents that only resided in the sand of the mold was increased above the top of the cope to prevent liquid metal from entering during filling. The filter was inaccessible with the current parting line so an extra cut into the mold was created so that the filter could be set in the drag and a separate piece of printed mold would be inserted into the bottom of the drag to hold the filter in place. Grips were added to both the cope and drag to make handling and assembling the mold more manageable. Each core, except for the center core, was printed and attached to the drag. In order to insert the chill, the center core was printed separate from the drag so that the one half of the chill could be placed in the drag. Then the center core was attached to the drag. Finally, the second half of the chill was placed inside the cope, Figure 3.11. The cope and drag were assembled with locators to assure the cope and drag aligned correctly. The mold CAD model was finished and sent to UNIMCC to be print in sand.

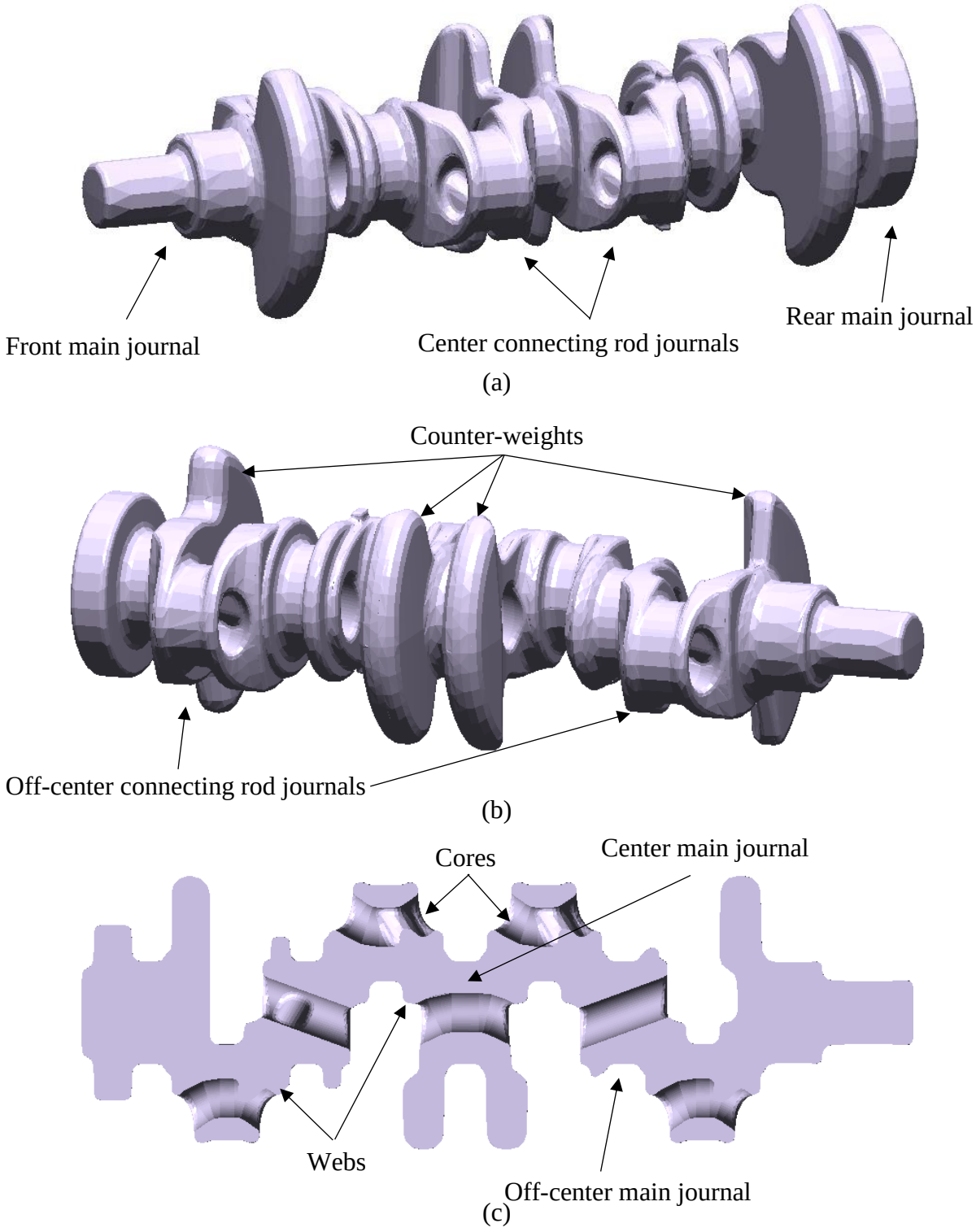

Figure 3.1 Geometry model of GM SGE cored crankshaft. (a) First isometric view, (b) second isometric view, (c) top view of a cut through the horizontal midplane. Various components of the crankshaft are labeled.

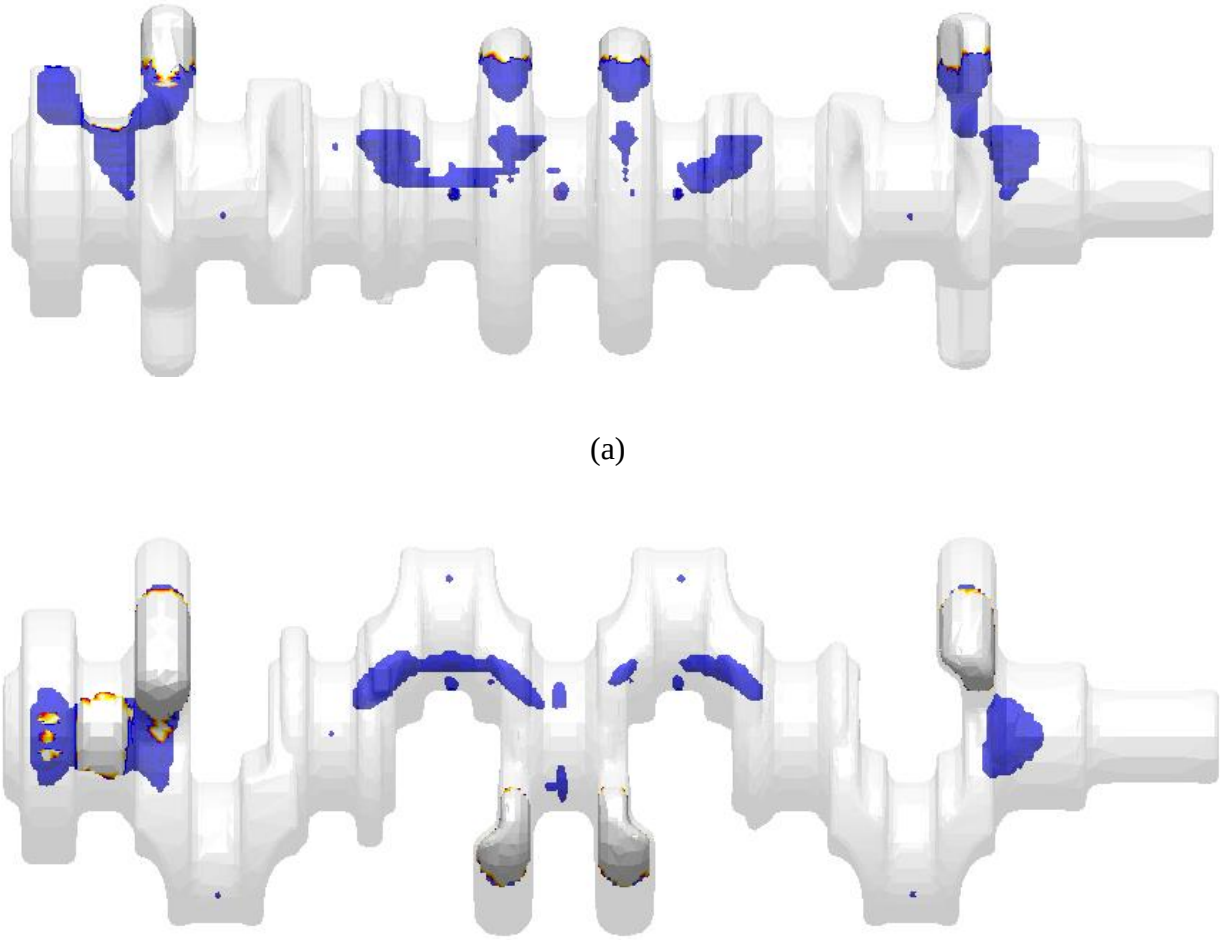

(a)

(b)

Figure 3.2 An x-ray (a) side and (b) top view of the crankshaft with no risers (natural solidification). The blue areas indicate locations of high porosity with in the crankshaft.

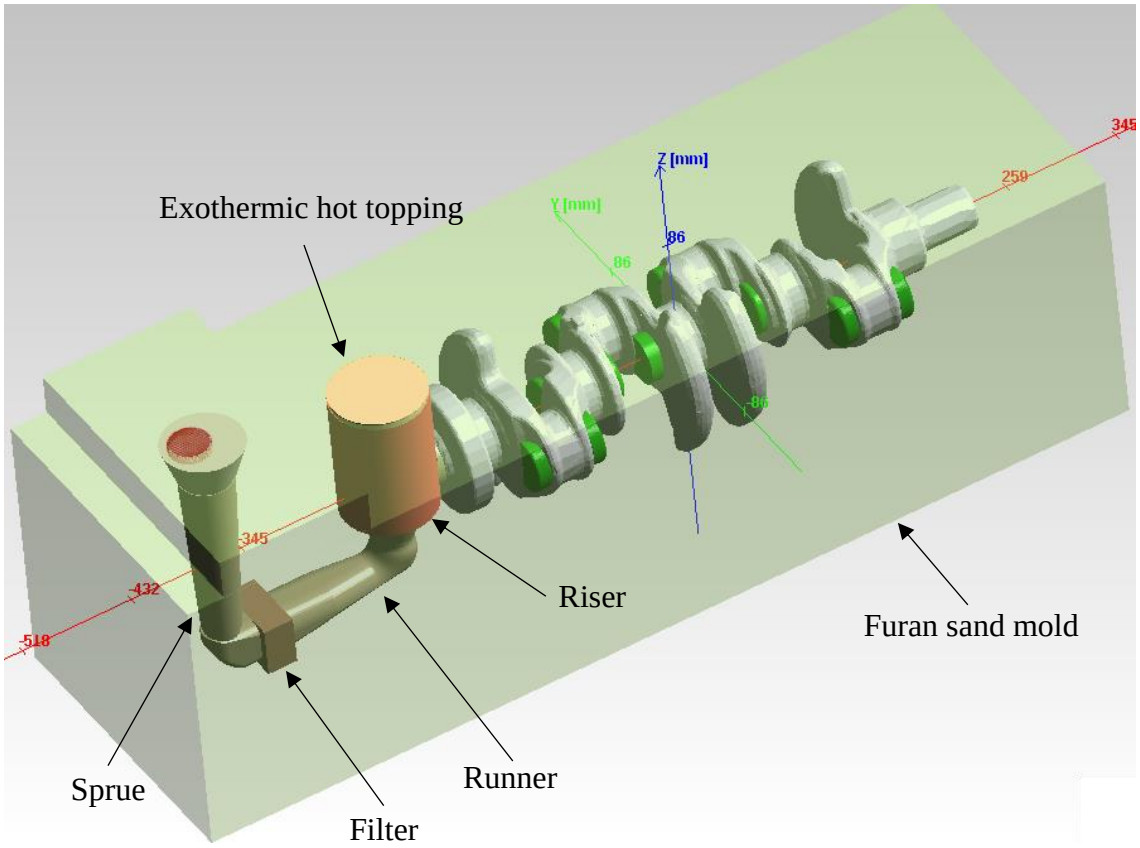

Figure 3.3 Gating system and riser added to the crankshaft. The crankshaft was filled from below the riser in front of the rear main journal.

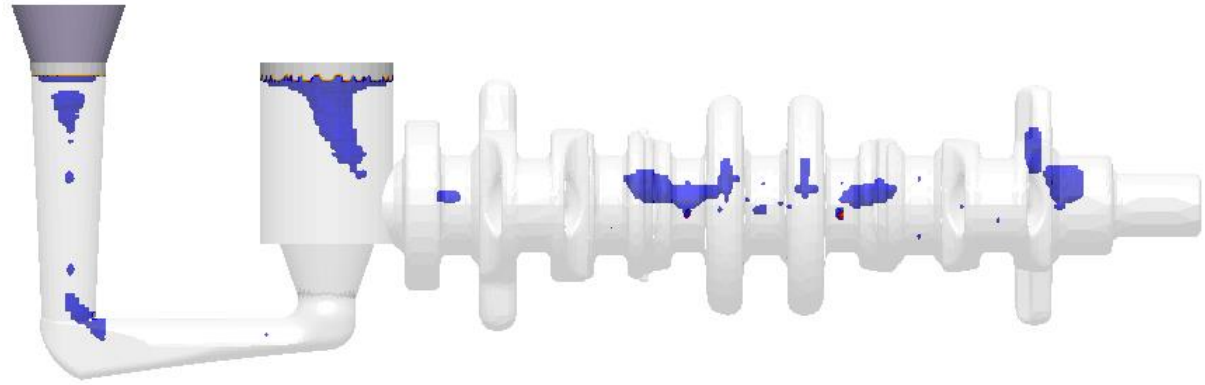

(a)

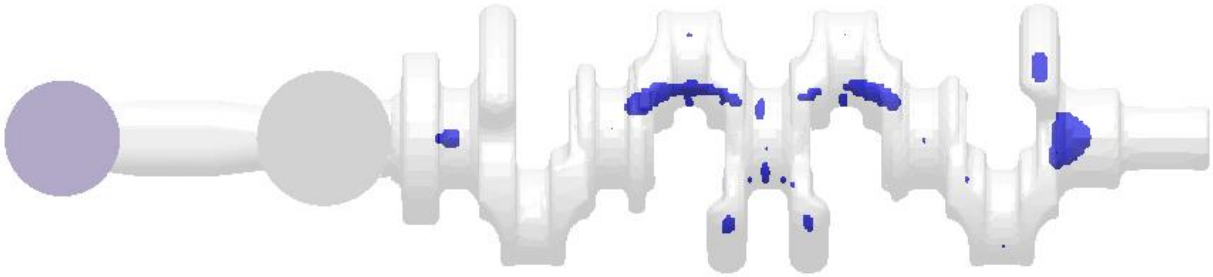

(c)

Figure 3.4 An x-ray (a) side and (b) top view of the crankshaft with one riser in front of the rear main journal. The blue areas indicate locations of high porosity with in the crankshaft.

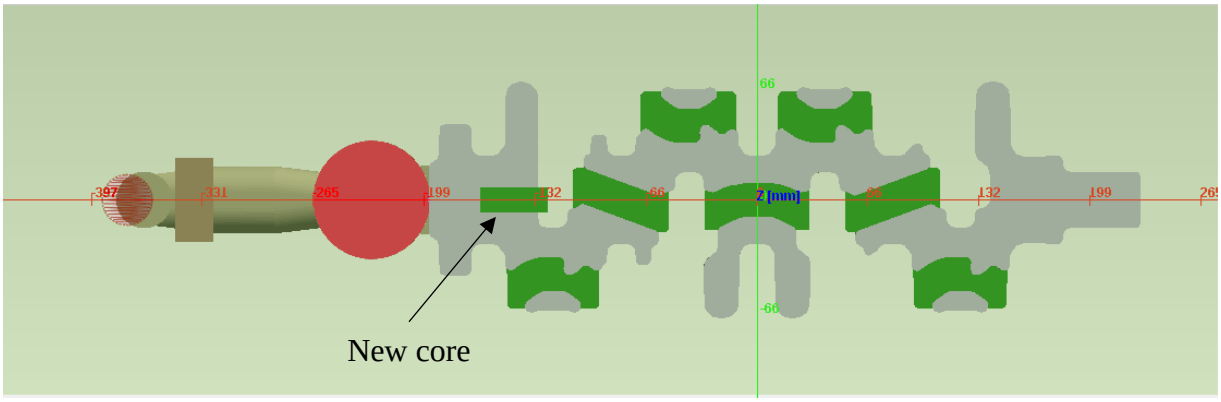

Figure 3.5 Crankshaft with new core in the rear main journal. Viewed from a horizontal midplane cut.

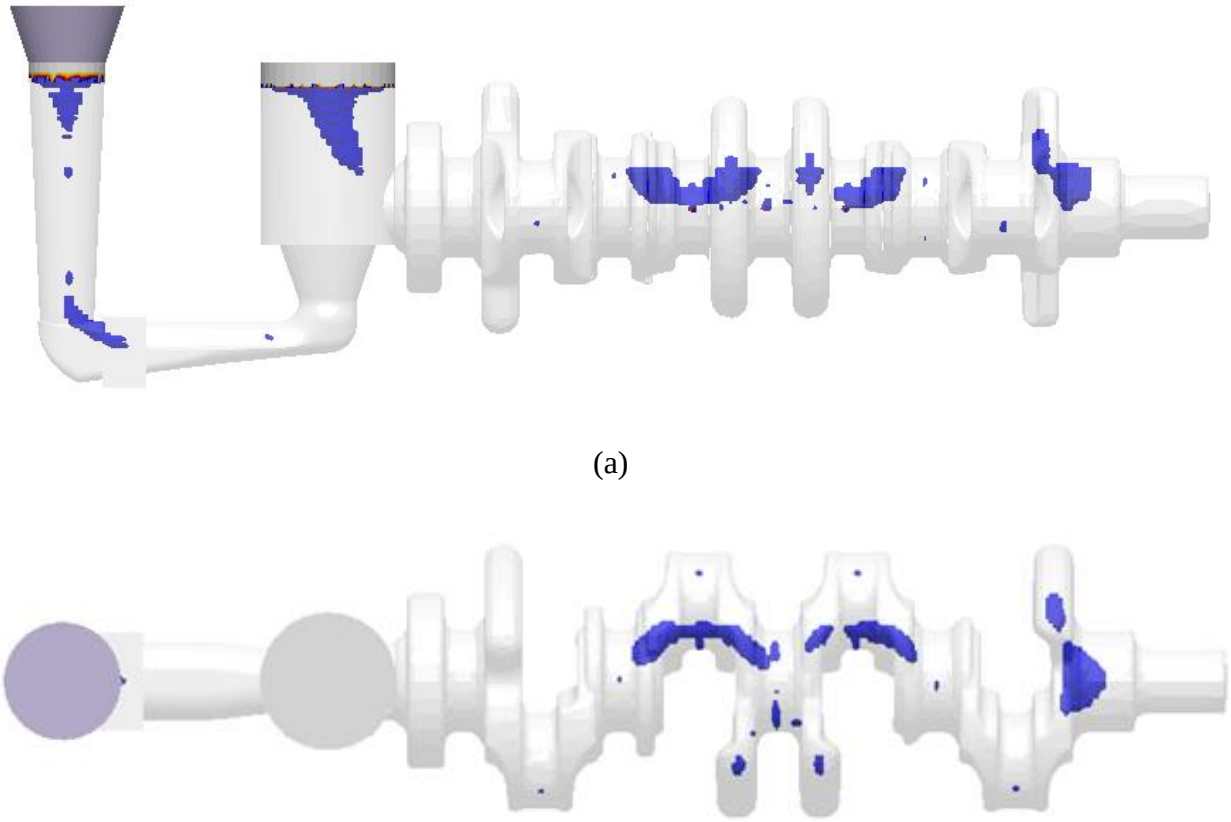

(a)

(b)

Figure 3.6 An x- ray (a) side and (b) top view of the crankshaft with one riser and a new core in the rear main journal. The blue areas indicate locations of high porosity with in the crankshaft.

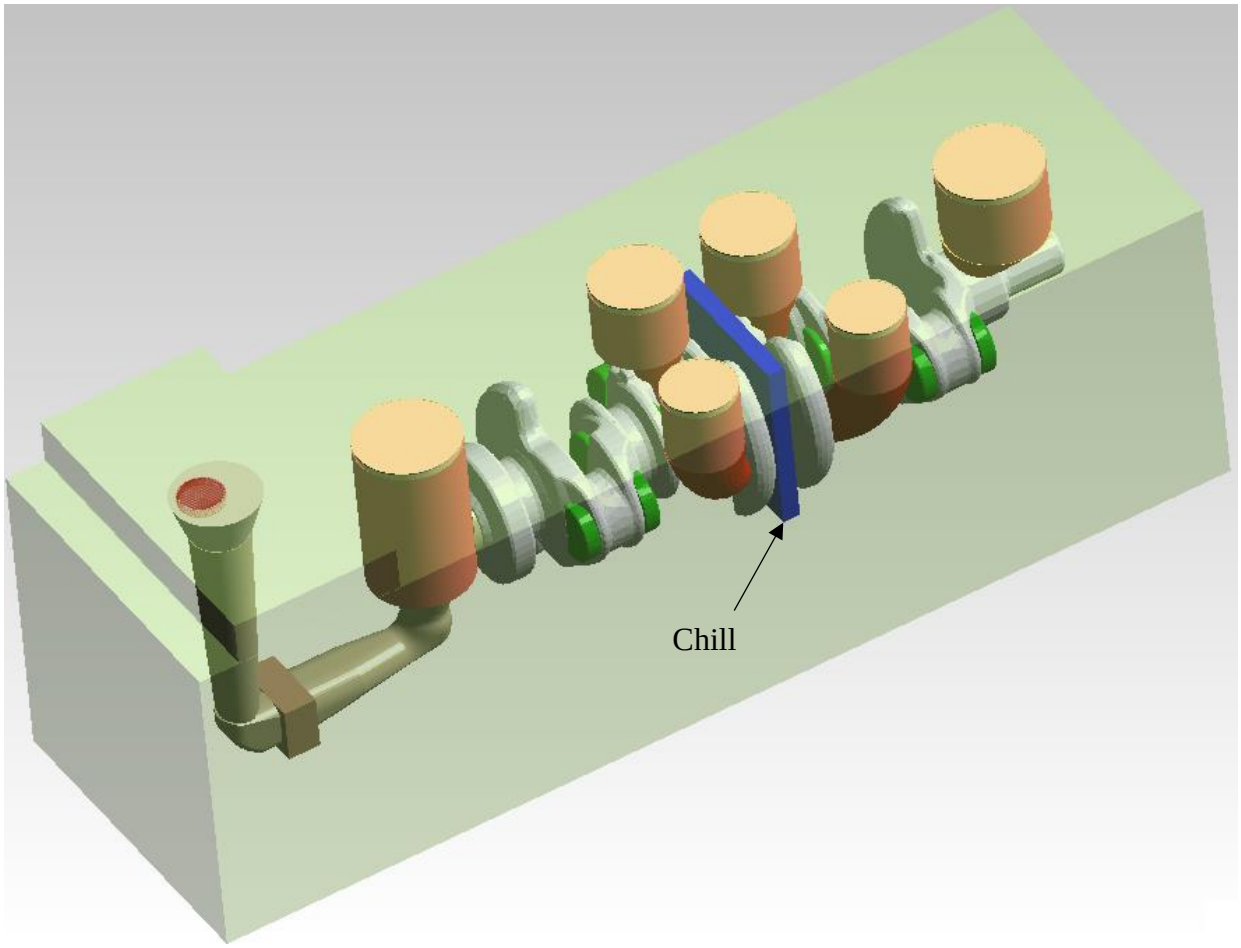

Figure 3.7 Completed gating and risering system for GM SGE crankshaft.

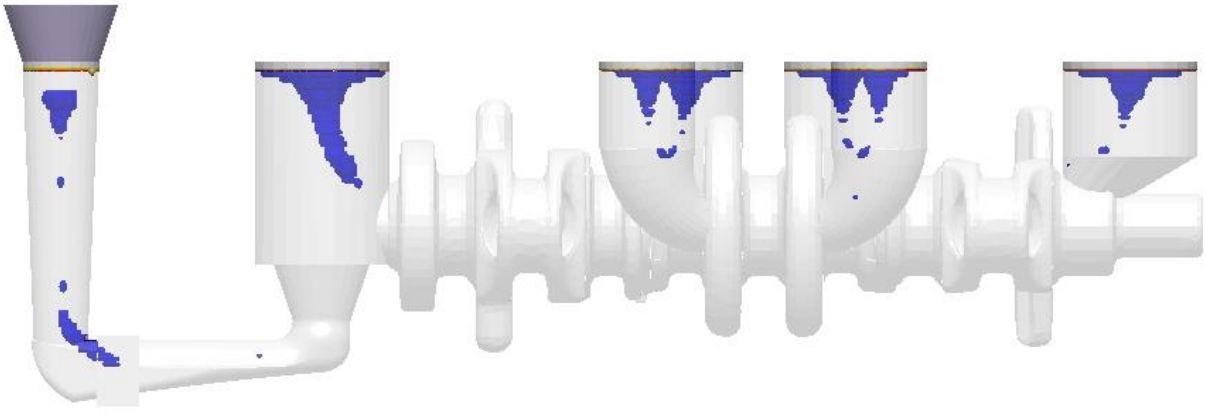

(a)

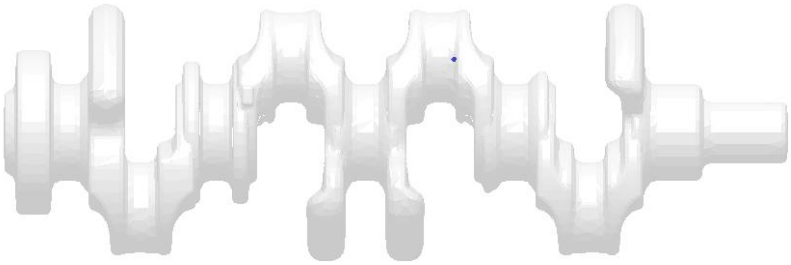

(b)

Figure 3.8 An x-ray (a) side and (b) top view of the crankshaft with six risers and a chill wrapped around the center main journal. The blue areas indicate locations of high porosity within the crankshaft.

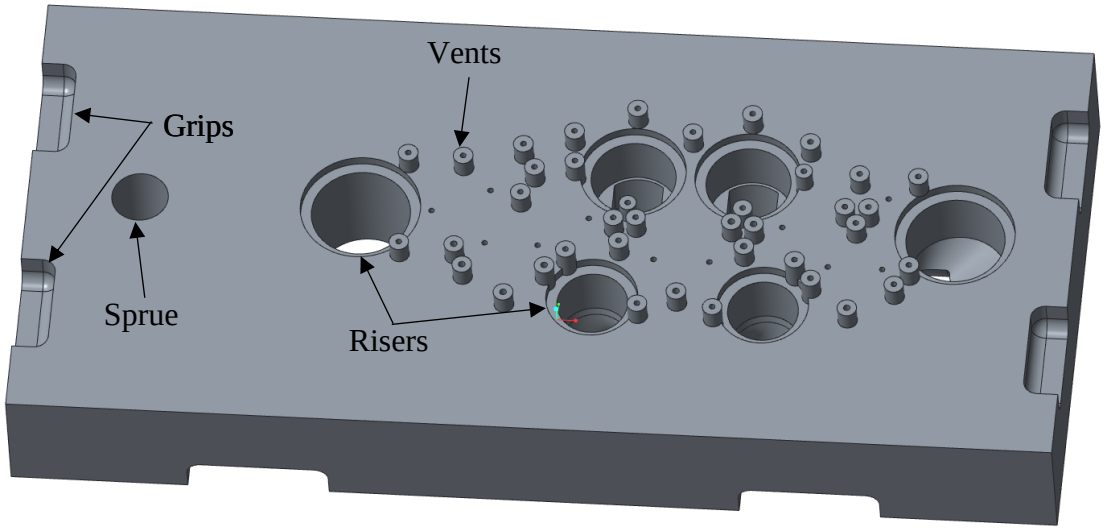

(a)

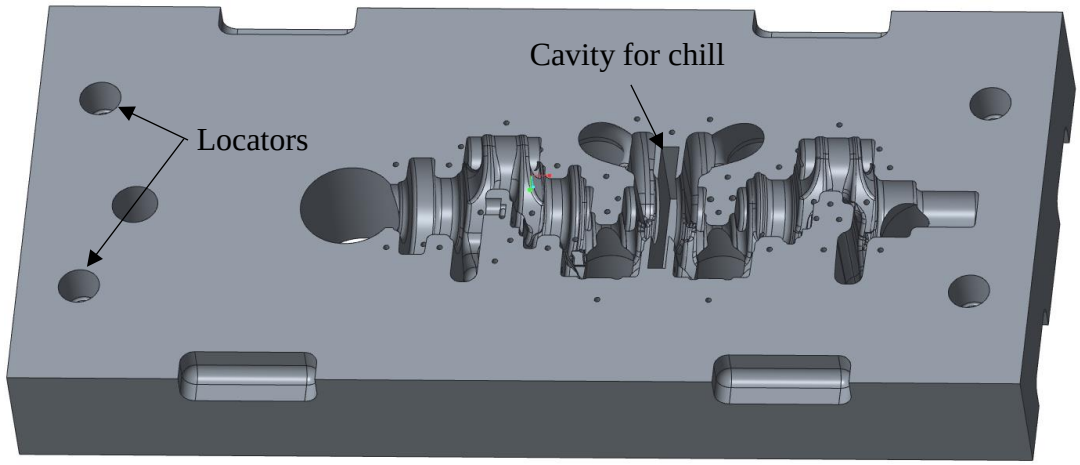

(b)

Figure 3.9 CAD model of the (a) top side and (b) bottom side of the cope.

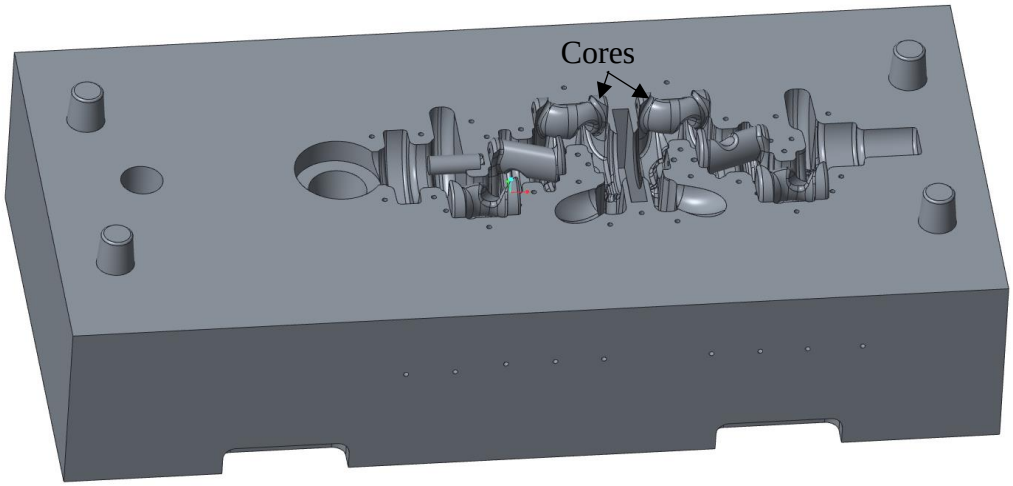

(a)

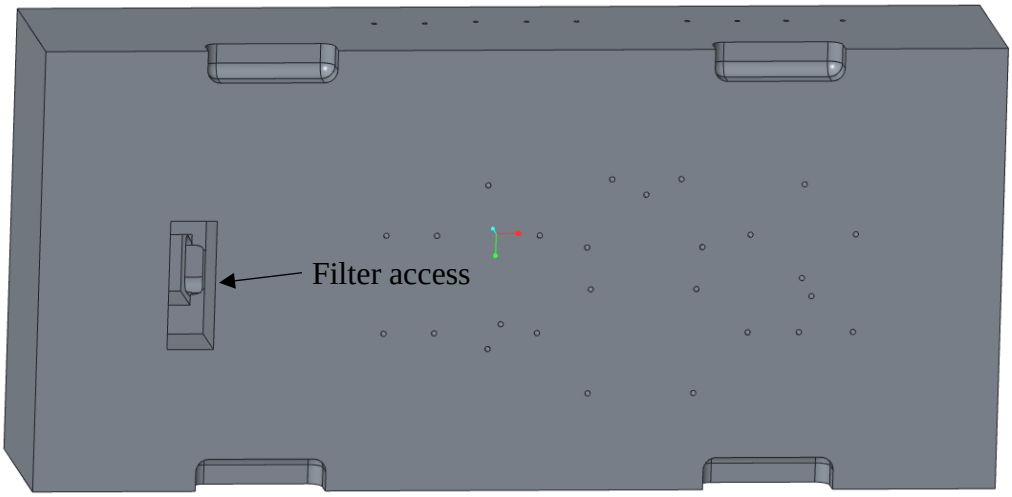

(b)

Figure 3.10 CAD model of the (a) top side and (b) bottom side of the drag.

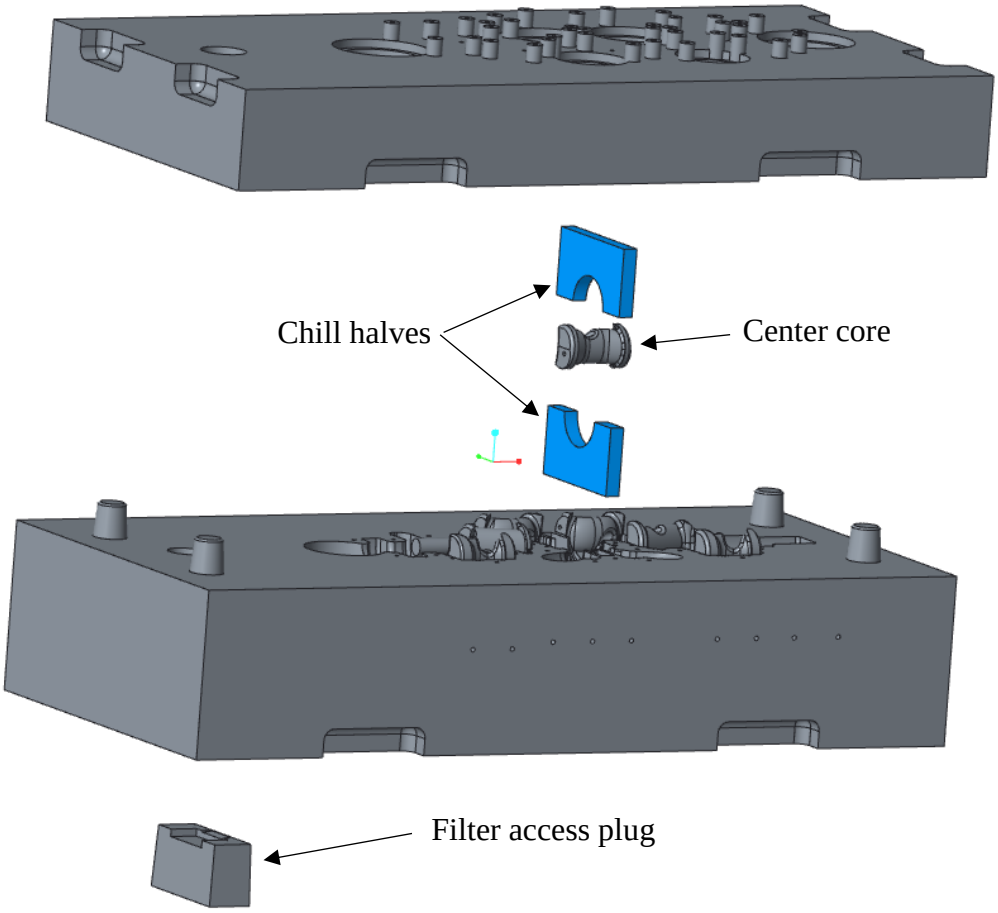

Figure 3.11 CAD model the mold assembly.

CHAPTER 4: PROTOTYPE CAST STEEL CRANKSHAFT

4.1 Introduction

Two 3D printed sand molds were printed for the prototype steel crankshaft rigging designed, and cast in a low alloy steel. The prototype crankshafts were inspected with x-ray images, dye penetrant [17], and microphotography for porosity. The results were compared directly to the porosity predicted by the simulations. From these comparisons, further improvements could be made to the crankshaft rigging.

4.2 Casting and Simulation

Two sand molds were created by the 3D printer at the UNICC, using the 3D model developed in Chapter 3. The two molds, shown in Figure 4.1, were brought to St. Louis Precision Casting Company to be cast. Prior to filling, both molds were assembled by placing the chill, filter, and middle core into their respective places. The molds were sprayed shown with an ethanol based mold wash. The cope and drag were sealed together with mold glue. Each mold was set within a steel brace and sand was packed between the outside of the mold and the steel brace's wall, to fortify the molds and prevent any liquid metal from leaking through the parting line onto the foundry floor. The ready-to-pour mold is shown in Figure 4.2.

At the foundry, St. Louis Precision Casting poured the castings directly from the furnace rather than using a ladle. The steel alloy chosen for the two castings was a low carbon alloy, which was developed by Caterpillar and General Motors as a potential alloy for cast steel crankshafts. The chemistry of the two crankshafts, shown in Table 4.1, was taken immediately before pouring the two molds. The molds were filled, without complications, and allowed to solidify. The castings

were removed from the molds placed into a sand blaster. The final two casting are shown in Figure 4.3.

Thermophysical properties were generated for the steel alloy composition, of the two cast steel crankshafts, which had been cast using the two 3D printed sand molds. These properties were generated using the *IDS Solidification Analysis Package for Steels* [18]. *IDS* software package inputs the steel alloy's element weight percent values, and calculates temperature dependent properties, such as density, thermal conductivity, specific heat, viscosity, and percent solid fraction. These were then uploaded to *MAGMAsoft* to re-simulate the filling and solidification of the GM SGE crankshaft rigging, which was identical to the two crankshafts cast. The simulated rigging included the vents for the casting and the cores to more closely match the cast crankshaft's rigging. The simulation geometry used is shown in Figure 4.4. The predicted porosity was directly compared to the results from Element Materials Technology (EMT).

4.3 Analysis of Macroporosity

The two cast crankshaft (referred to as Crankshaft 1 and Crankshaft 2) were sent to EMT for digital radiographic inspection, dye penetrant tests, and microphotography. Radiographs were taken before and after the risers were removed from the crankshaft. Comparison between the radiographic images and the predicted porosity results of the simulated casting for the crankshafts with the risers attached are shown in Figures 4.5-4.8. In these figures, EMT marked indication on the radiographs that were believed to be porosity, in the predicted porosity images approximately the same location was marked for comparison.

In general, the indications marked on the radiographs of the crankshafts with the risers attached do not closely match locations of predicted internal porosity (shown in blue in the figures).

However, the funnel shaped porosity in the risers, so called riser pipes, in the radiographs and corresponding porosity predictions are in good agreement.

The risers were removed and several more x-ray images were taken of the crankshafts. With the risers removed, more porosity indications in the crankshaft were revealed. The radiographs of the crankshafts with the riser removed are compared to the simulated porosity in Figures 4.9-4.10.

In order to get a clear understanding of the radiograph indications, each indication was assigned two numbers. The first number represented which crankshaft the indication was found on. The second number represented the location on the crankshaft where the indication was found. If an indication appeared in a similar location on both crankshafts, it was given the same second number. With this indication nomenclature, it was possible to recognize locations on the crankshaft rigging that required improvement i.e. locations where indications were present in both crankshafts. The indications were marked on the simulated crankshaft at the same location they are found in the radiographs.

The comparison of the radiographs and simulated crankshafts, show that Indications 1-2, 2-2, and 2-9 correlate to the macroporosity predicted within the center pin riser necks, near the crankshaft surface. This suggested that those risers were not able to completely feed the part below. Indication 1-3 did not relate to the prediction and based on the shape of the indication was believed to be a shadow created by the x-ray. Indication 1-4 was directly below a casting vent. If the vent become blocked during filling, the air displaced in the mold cavity by the rising liquid steel could have become trapped in the casting. Indication 2-10 did not appear in the simulated crankshaft and it was unclear the reason this porosity formed. Both the macro and micro porosity predictions show very low levels of porosity at the same location as Indication 2-10. The remaining indications

could not be explained by comparison to the simulated macroporosity. Therefore, a closer inspection of the crankshaft's porosity was necessary.

4.4 Analysis of Microporosity

Crankshaft 1 was halved along the horizontal centerline and one half was partitioned into three sections. A dye penetrant test was performed on the face of each section. The results of the dye penetrant tests were compared to the microporosity predicted at the same locations by the *MAGMAsoft* simulation, and are shown in Figures 4.11-4.13. The technician indicated several likely pores in the dye penetrant images. In Figures 4.11 and 4.13, the likely pore locations are in areas of relatively high predicted porosity. In Figure 4.12, the likely pore locations were all in areas of relatively low porosity.

The three midplane sections of the crankshaft were cut into fourteen different samples, which are outlined red in Figure 4.14, and were given a high polish. EMT quantified the porosity percentage of the surface by capturing hundreds of microphotographs. The microphotographs were combined to recreate the entire surface of each sample at fifty times magnification, rendering the microporosity in each sample visible. It was not explicitly clear how EMT calculated the percentage porosity for each sample. Two polished samples, which are labeled Sample 1 and 2 in Figure 4.14, were chosen for verification, which is shown in the following section. The percentage porosity that was reported by EMT for each sample is shown Figure 4.14 as the top percentage listed near its respective sample. An approximated location of the field with maximum porosity is represented by a white dot within each sample on Figure 4.14. That field's porosity percentage is shown in parenthesis below the percentage porosity of the entire sample. In general, the reported locations of maximum porosity in each sample are located in the same proximity as locations of

high levels of predicted porosity. The reported percentage porosity values are in good agreement with the predicted values.

In the previous section, some of the indication present on the x-ray images could not be fully explained by the macroporosity predictions. The contour of predicted microporosity in Figure 4.14 was overlaid with several indications from the radiographs in relatively the same locations. From this combination of inspection methods, it was found that Indications 1-1 and 2-1, which were present on all four x-ray images, were related to the higher levels of predicted microporosity located around the exterior of the rear main journal. Indications 1-5, 1-6, 2-7, 2-8, and 2-11 are all adjacent to cores where high levels of microporosity was predicted. Overall, the prototype crankshafts contained relatively low levels of porosity, due in part to a well-designed rigging system for which the simulated porosity is in good agreement with the cast crankshaft analyses.

4.5 Verification of Reported Microporosity

In order to verify the porosity reported on the sample surfaces, two polished samples (referred to as Sample 1 and Sample 2) were chosen, shown in Figure 4.15, due to the relatively high range of predicted porosity levels of each sample. A petrographic microscope was used to take dozens of four-times-magnified, high-resolution images of the polished surface of Sample 1 and 2. An example of one of the many images is shown in Figure 4.16. The individual images were digitally merged, or stitched, together to form one complete high-resolution image of the sample surface, which are shown in Figure 4.17.

In order to quantify the porosity on the sample surfaces the image processing software *ImageJ* [19] was used to converted the stitched images into the black and white binary images shown in Figure 4.18. In the binary image, black pixels represented porosity and white pixels represented a clean sample surface. The binary image is created by setting the stitched images to

a grayscale color scheme, where each pixel can be represented on a scale from 0 to 255, with 0 being black and 255 representing white. A threshold filter is applied to the image so that all pixel values below 90 are changed to 0 (black) and all the pixel values above are changed to 255 (white). The value for the threshold was chosen because it best captured the porosity in the image without also converting shadows in the image to pixel value 0. The percent porosity for the entire sample surface was found by dividing the number of black pixels by the number of white pixels. These results were compared to the reported porosity levels in Table 4.2.

EMT reported a percentage porosity of 0.1% for Sample 1 and 0.01% for Sample 2. The binary images percentage porosity was found to be 0.09% for Sample 1 and 0.06% for Sample 2. The difference between the reported and binary image porosity can be explained by the threshold level chosen, varying the threshold affected the porosity present in the binary image. However, the initial results were sufficient for verifying the reported porosity levels.

In order to compare the prototype casting to the simulated casting, contours of the percentage porosity were generated from the binary images. First, the binary images were deconstructed into the two images shown in Figure 4.19 for Sample 1. In the first image the black background was removed so the porosity was the only black pixels. The second image represents a mask of the sample where the sample surface has a pixel value of 0 and the background is 255. The two images were broken down into the 600 by 600 pixel grid spaces shown in Figure 4.20. Then the percentage of black pixels in each grid space was found for the two images. In the binary image without a background, the percentage value represented the fraction of porosity present in each grid space, $\mathbf{A_p}$. In the mask image, the percentage value represented the fraction of the grid space that contained the sample $\mathbf{A_s}$. By dividing $\mathbf{A_p}$ by $\mathbf{A_s}$ and multiplying by 100% the percentage porosity was found for each grid space. The percentage porosity for each grid space was exported

to the graphing software *TecPlot*, and contours of the percentage porosity for each sample was generated and directly compared to the predicted porosity at the same location in Figures 4.21-4.22. The predicted porosity contours did not exactly match the contours from the binary images. However, the magnitude of the porosity in both sets of contours was similar.

Figure 4.1 Cope and drag of one of the two sand molds used to cast the prototype steel crankshaft.

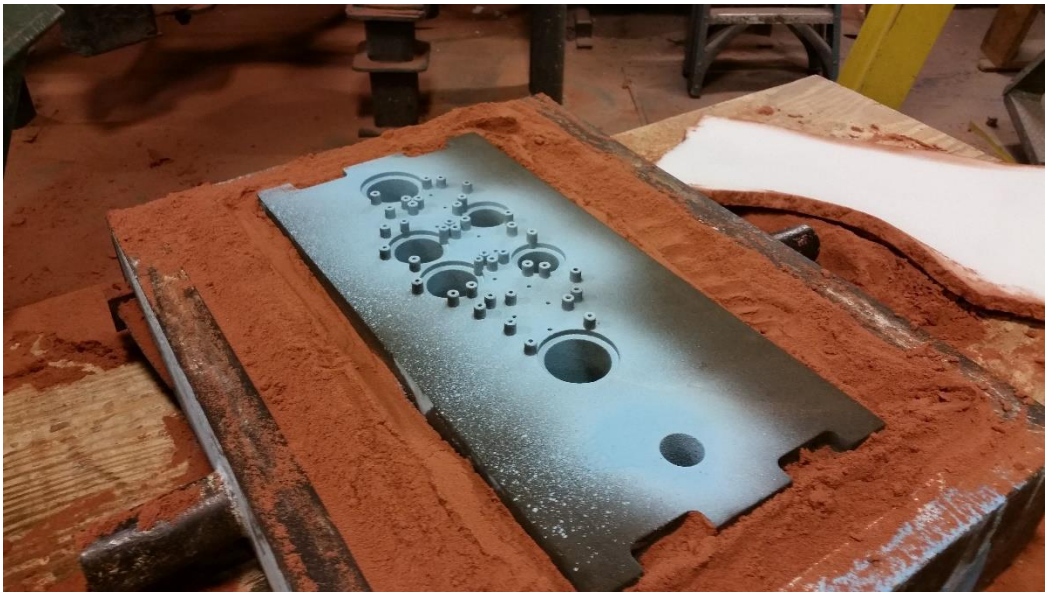

Figure 4.2 One of two molds, surrounded by packed sand in a flask, before filling.

Table 4.1 Chemistry composition of the two prototype cast steel crankshafts.

Element	%	Element	%
C	0.33	**Nb**	0.0029
Si	0.398	**V**	0.099
Mn	1.38	**W**	0.015
P	0.017	**Pb**	0.0035
S	0.021	**B**	0.0024
Cr	0.333	**Sn**	0.027
Ni	0.094	**Zn**	0.0015
Mo	0.23	**Bi**	<0.0015
Al	0.071	**Ca**	0.0051
Cu	0.117	**Ce**	<0.0020
Co	0.0022	**N**	0.012
Ti	0.0022		

(a)

(b)

Figure 4.3 Top view of Crankshaft 1 and side view of Crankshaft 2 with rigging still attached.

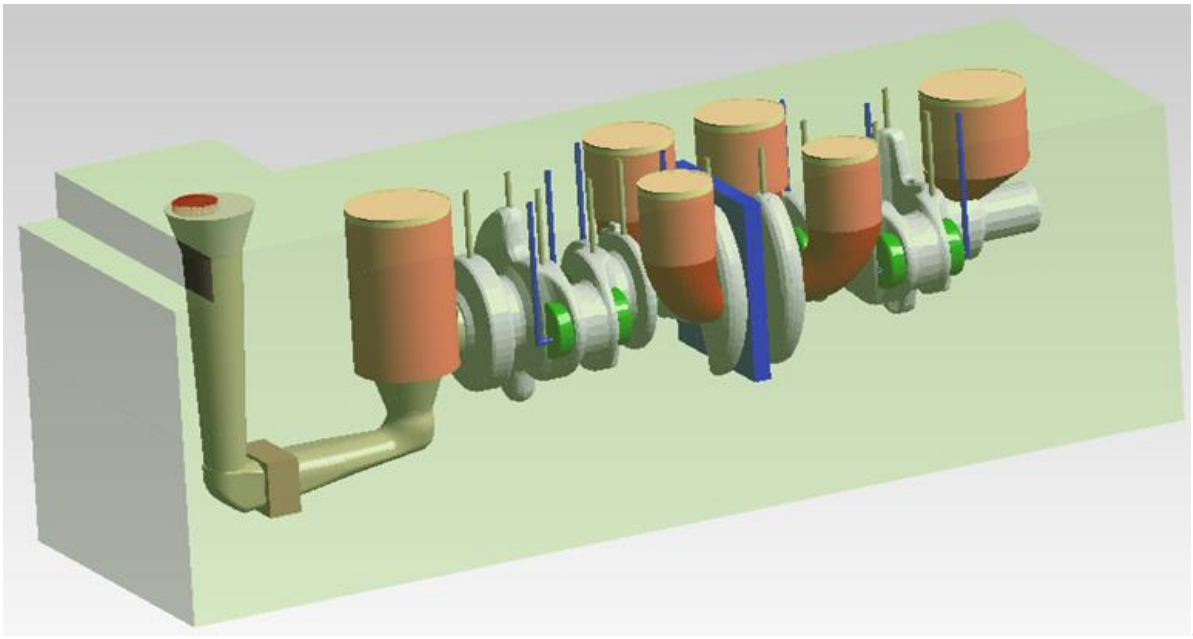

Figure 4.4 Simulation geometry of the prototype cast steel crankshaft.

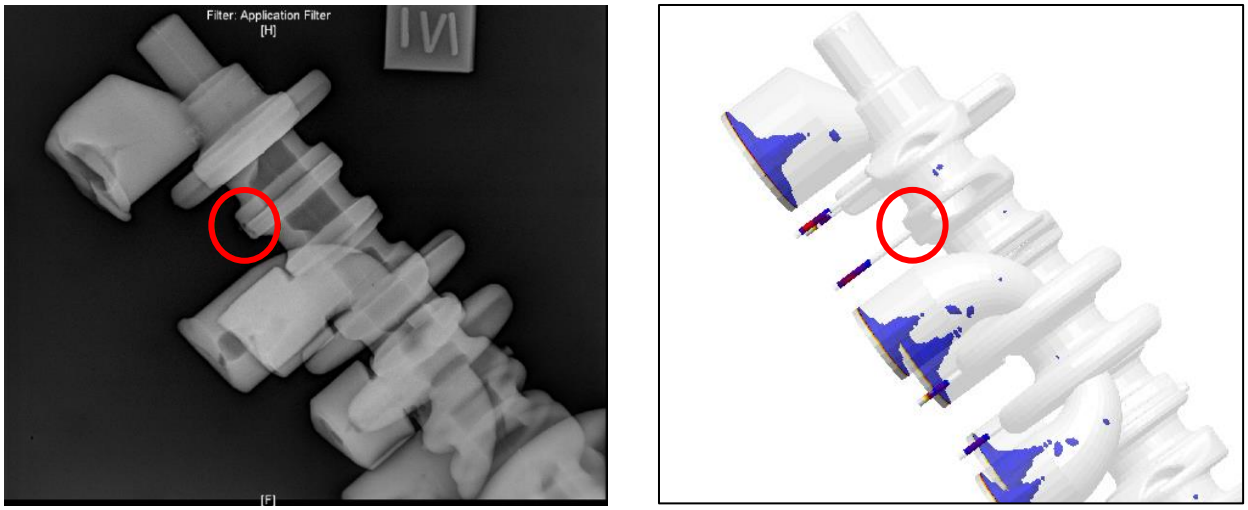

(a) (b)

Figure 4.5 Comparison of (a) the first radiograph view of Crankshaft 1 and (b) the simulated crankshaft. Red circle in (a) was labeled as a gas hole/porosity. The same location is marked in (b). Blue areas in (b) indicate predicted porosity within the crankshaft.

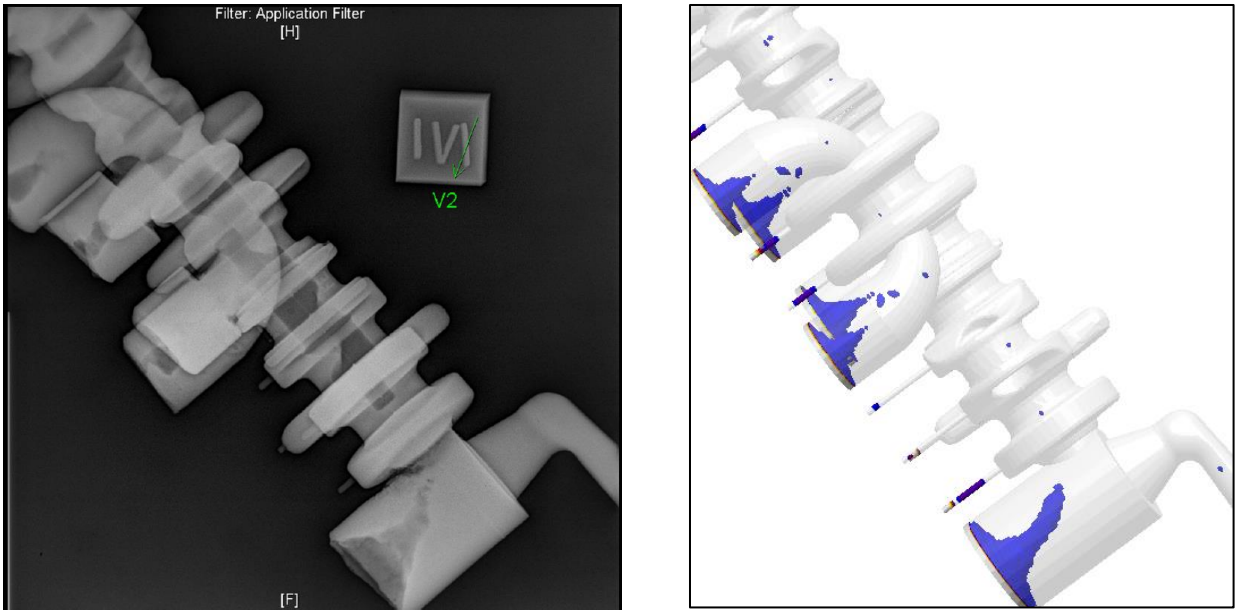

(a) (b)

Figure 4.6 Comparison of (a) the second radiograph view of Crankshaft 1 and (b) the simulated crankshaft. No defect was indicated. Blue areas in (b) indicate predicted porosity within the crankshaft.

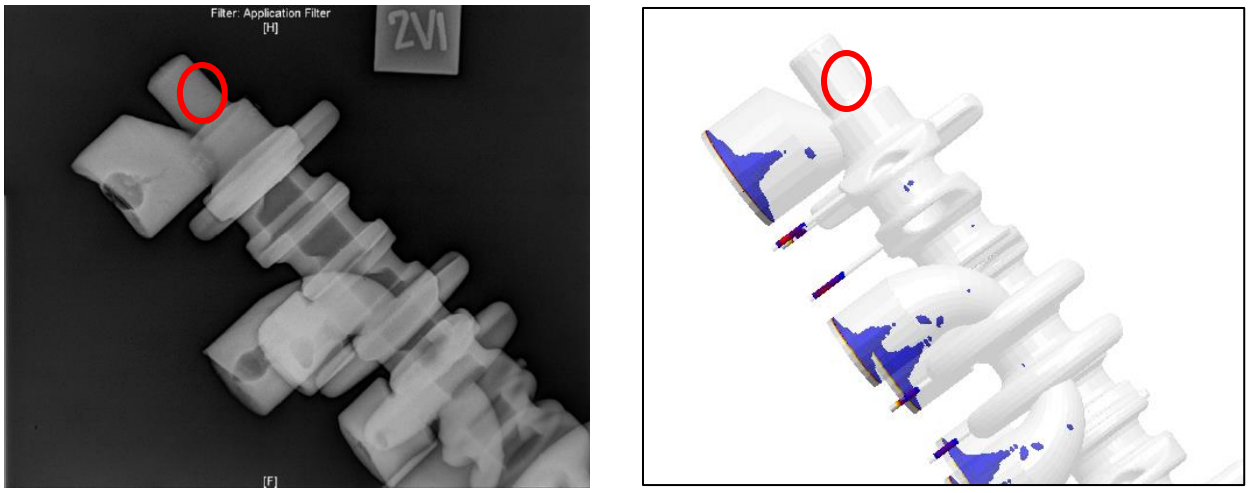

(a) (b)

Figure 4.7 Comparison of (a) the first radiograph view of Crankshaft 2 and (b) the simulated crankshaft. Red circle in (a) was labeled as a shrinkage cavity. The same location is marked in (b). Blue areas in (b) indicate predicted porosity within the crankshaft.

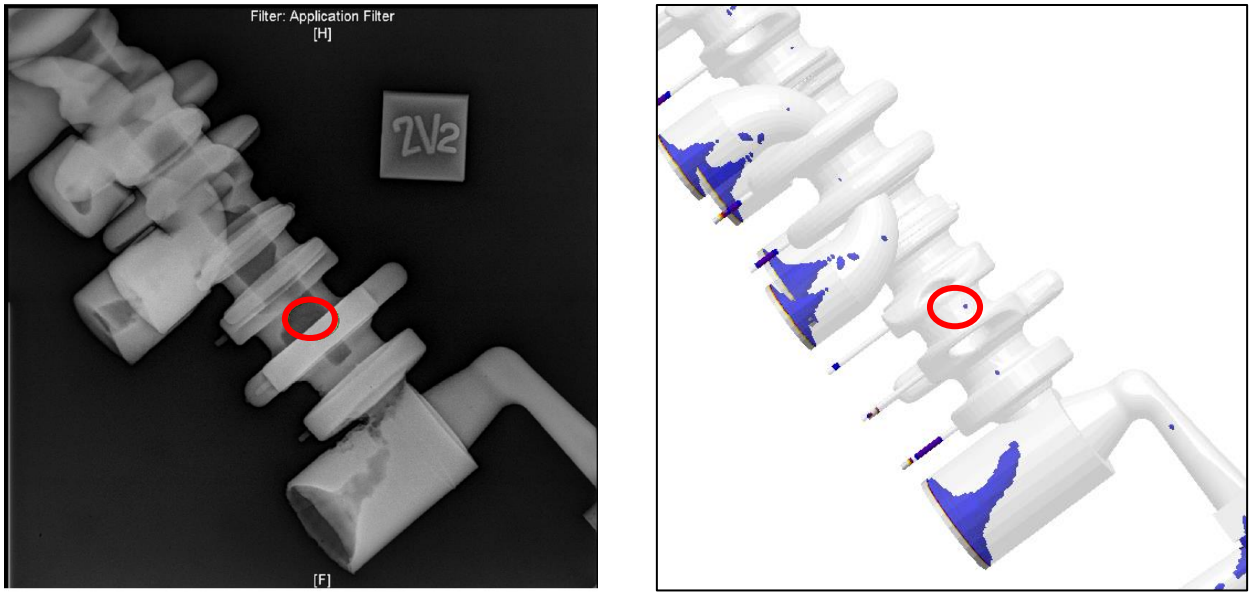

(a) (b)

Figure 4.8 Comparison of (a) the second radiograph view of Crankshaft 2 and (b) the simulated crankshaft. Red circle in (a) was labeled as a shrinkage cavity. The same location is marked in (b). Blue areas in (b) indicate predicted porosity within the crankshaft.

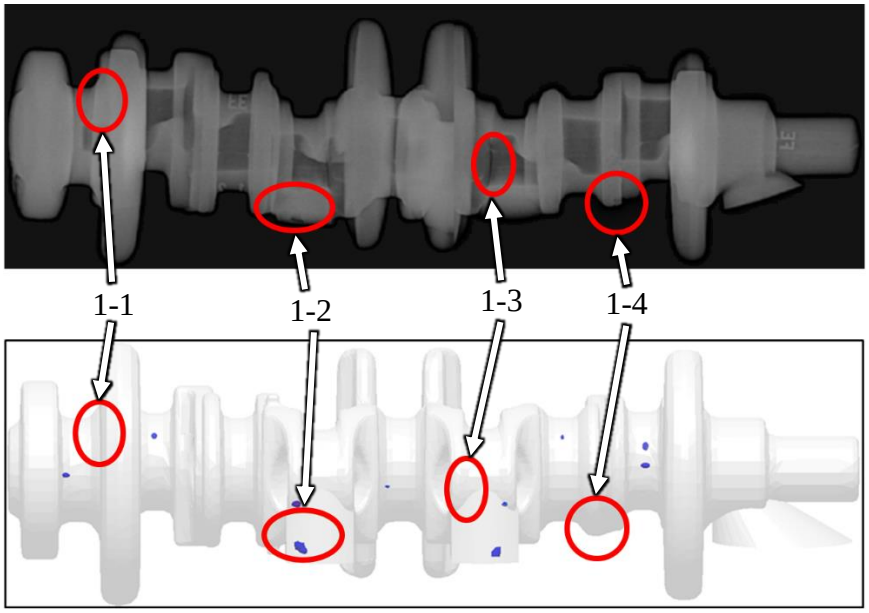

(a)

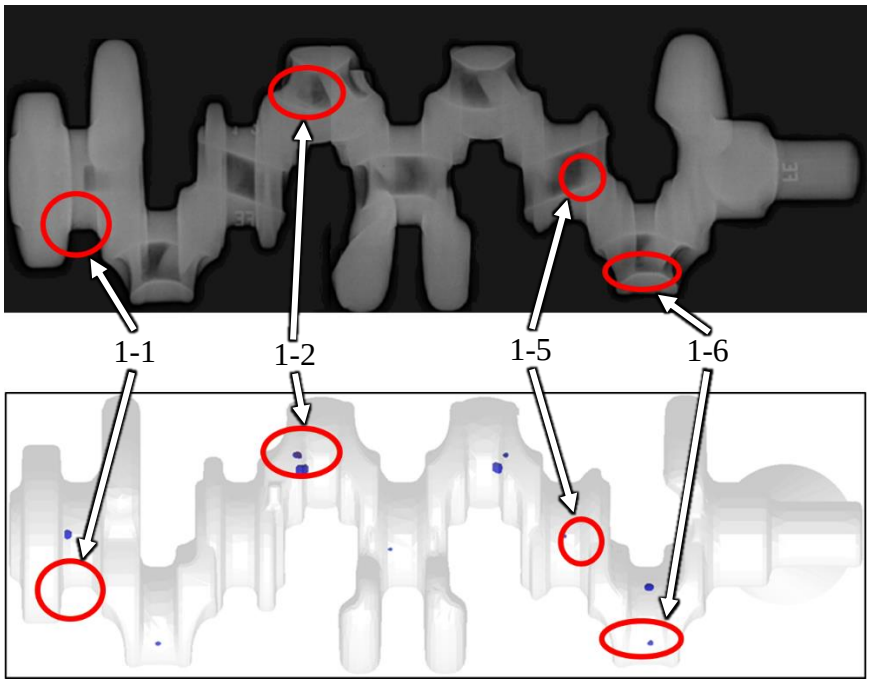

(b)

Figure 4.9 Comparison between x-ray images and predicted porosity of the prototype crankshaft with the risers removed. (a) Side view Crankshaft 1, (b) top view of Crankshaft 1. Red circles in the radiograph indicate a defect marked by the technician. The same locations are marked in the simulated crankshaft. Blue areas indicate predicted porosity within the crankshaft.

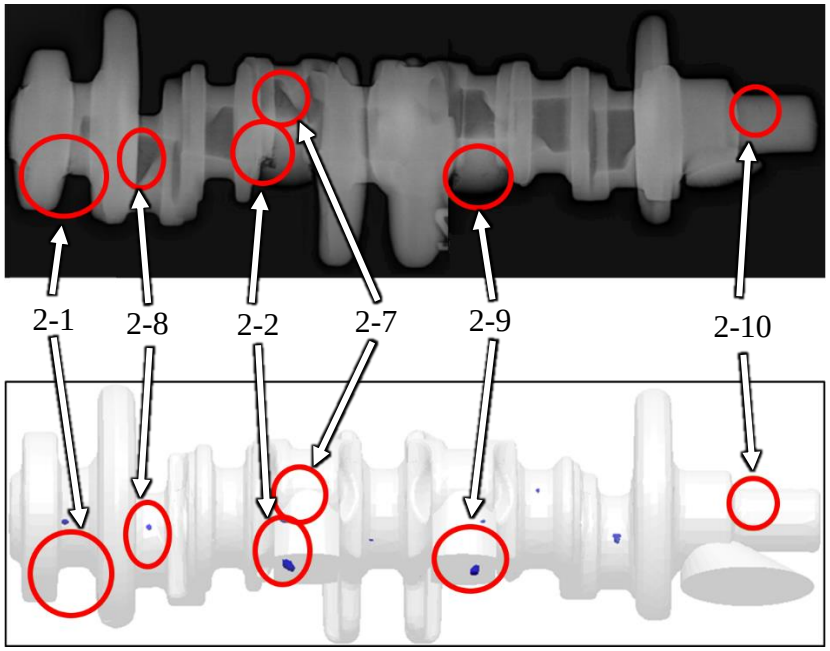

(a)

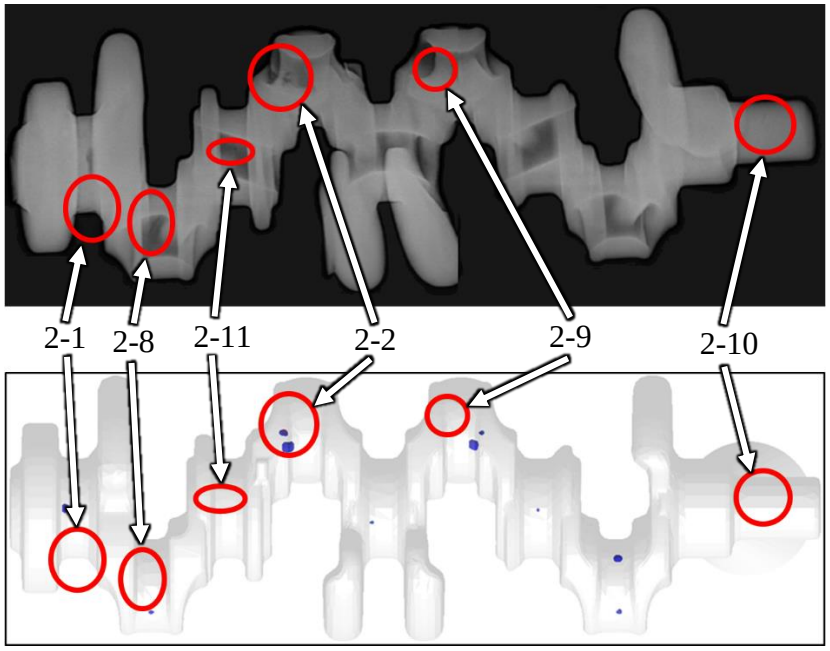

(b)

Figure 4.10 Comparison between x-ray images and predicted porosity of the prototype crankshaft with the risers removed. (a) Side view Crankshaft 2, (b) top view of Crankshaft 2. Red circles in the radiograph indicate a defect marked by the technician. The same locations are marked in the simulated crankshaft. Blue areas indicate predicted porosity within the crankshaft.

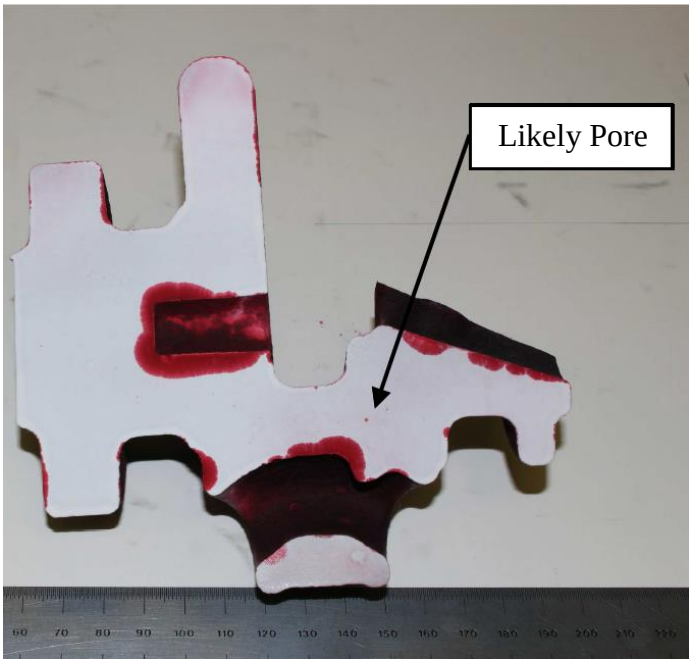

(a)

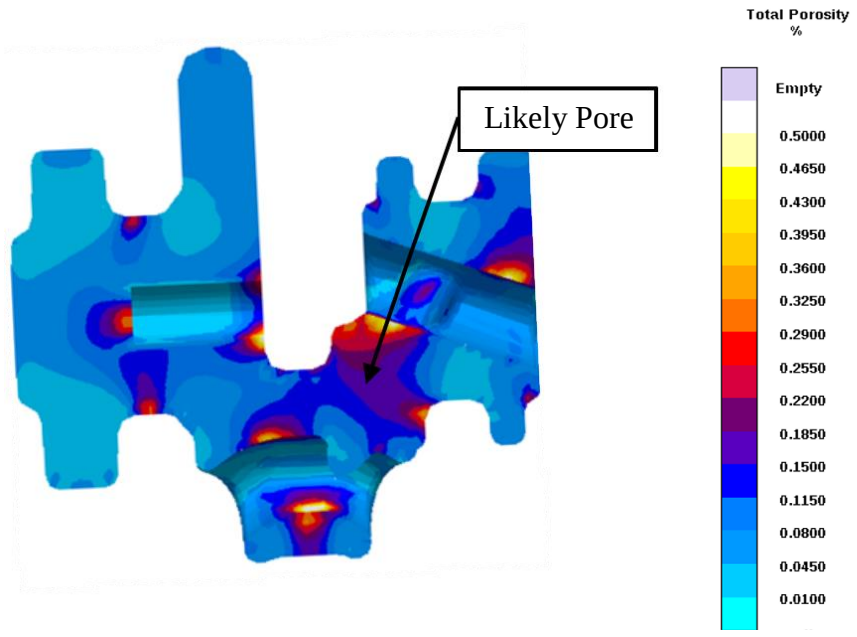

(b)

Figure 4.11 Porosity comparison between the rear section of the (a) dye penetrant test of Crankshaft 1 and (b) the simulated crankshaft. Element indicated locations of likely porosity. The same location is marked in (b).

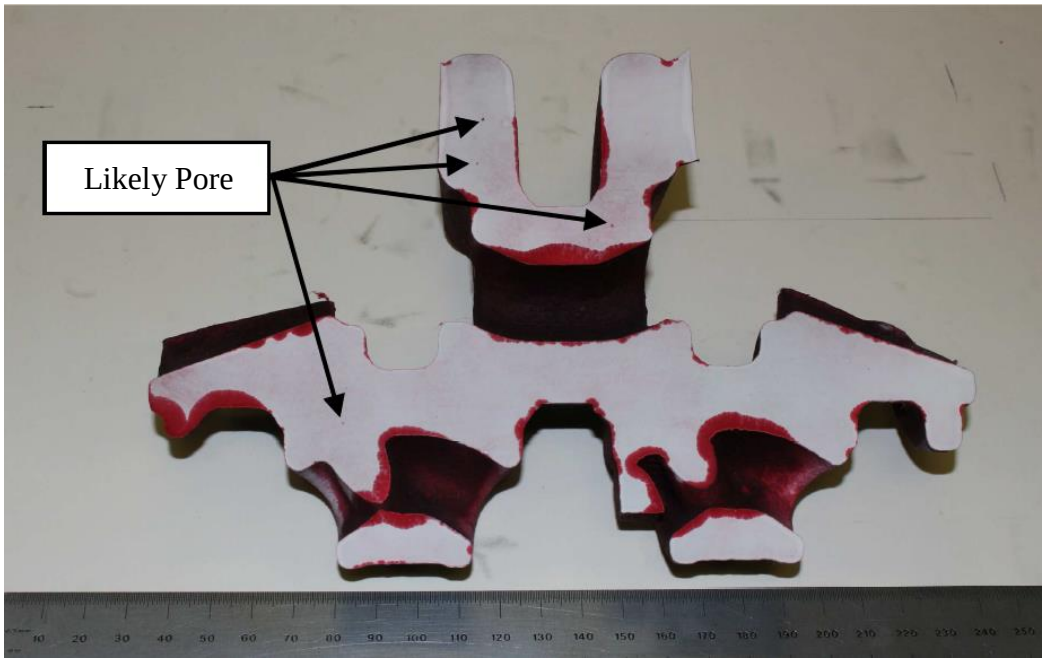

(a)

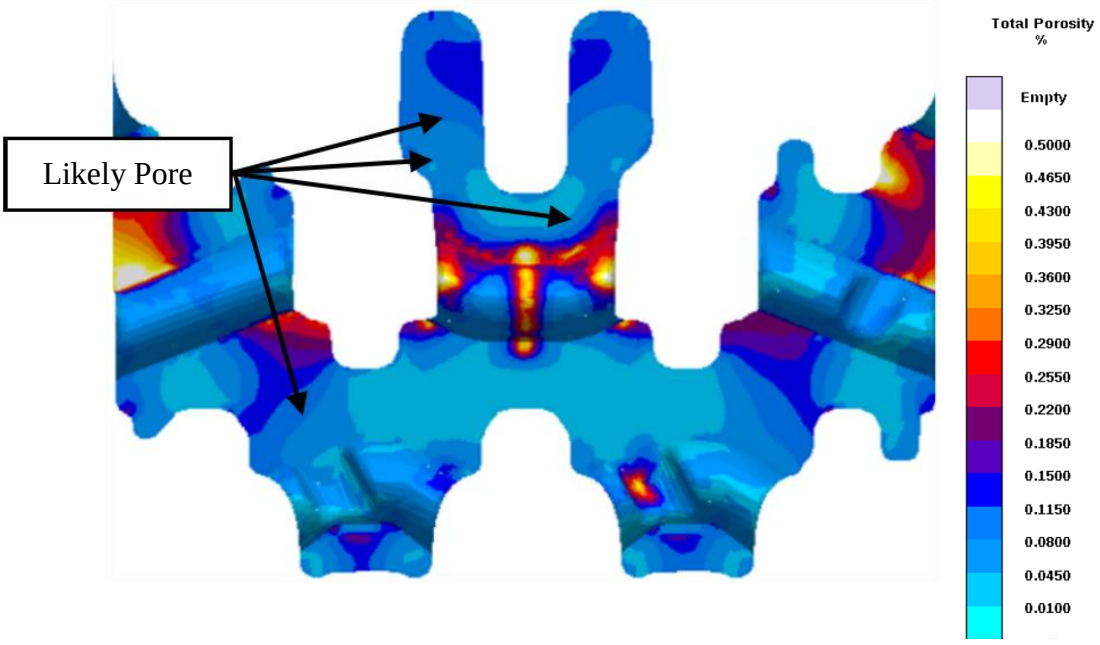

(b)

Figure 4.12 Porosity comparison between the center section of the (a) dye penetrant test of Crankshaft 1 and (b) the simulated crankshaft. Element indicated locations of likely porosity. The same location is marked in (b).

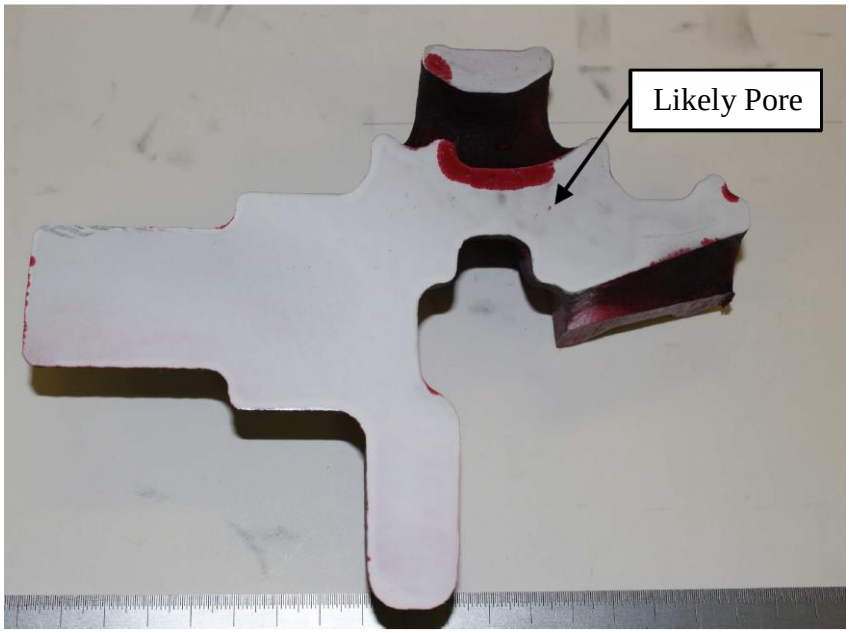

(a)

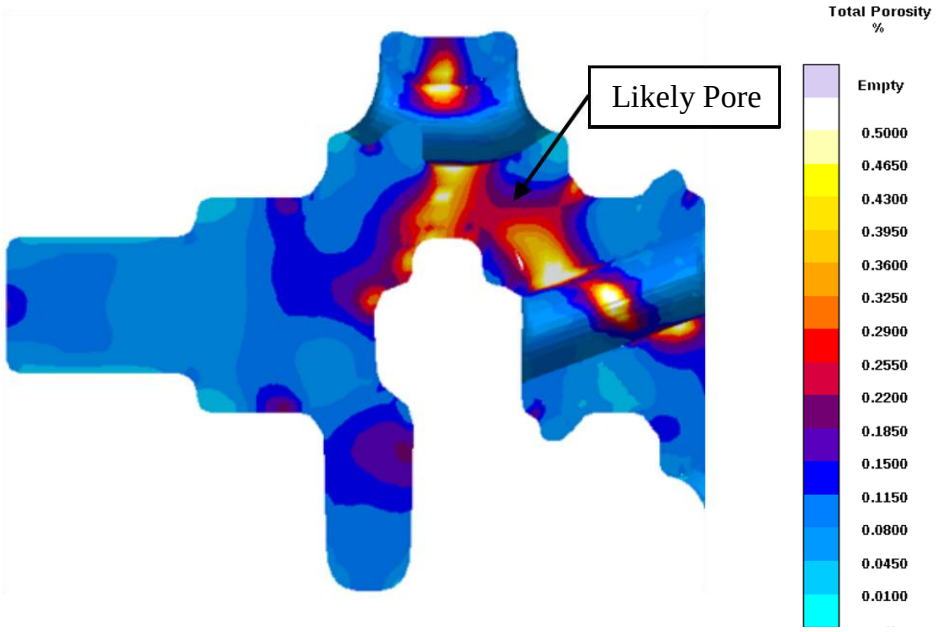

(b)

Figure 4.13 Porosity comparison between the front section of the (a) dye penetrant test of Crankshaft 1 and (b) the simulated crankshaft. Element indicated locations of likely porosity. The same location is marked in (b).

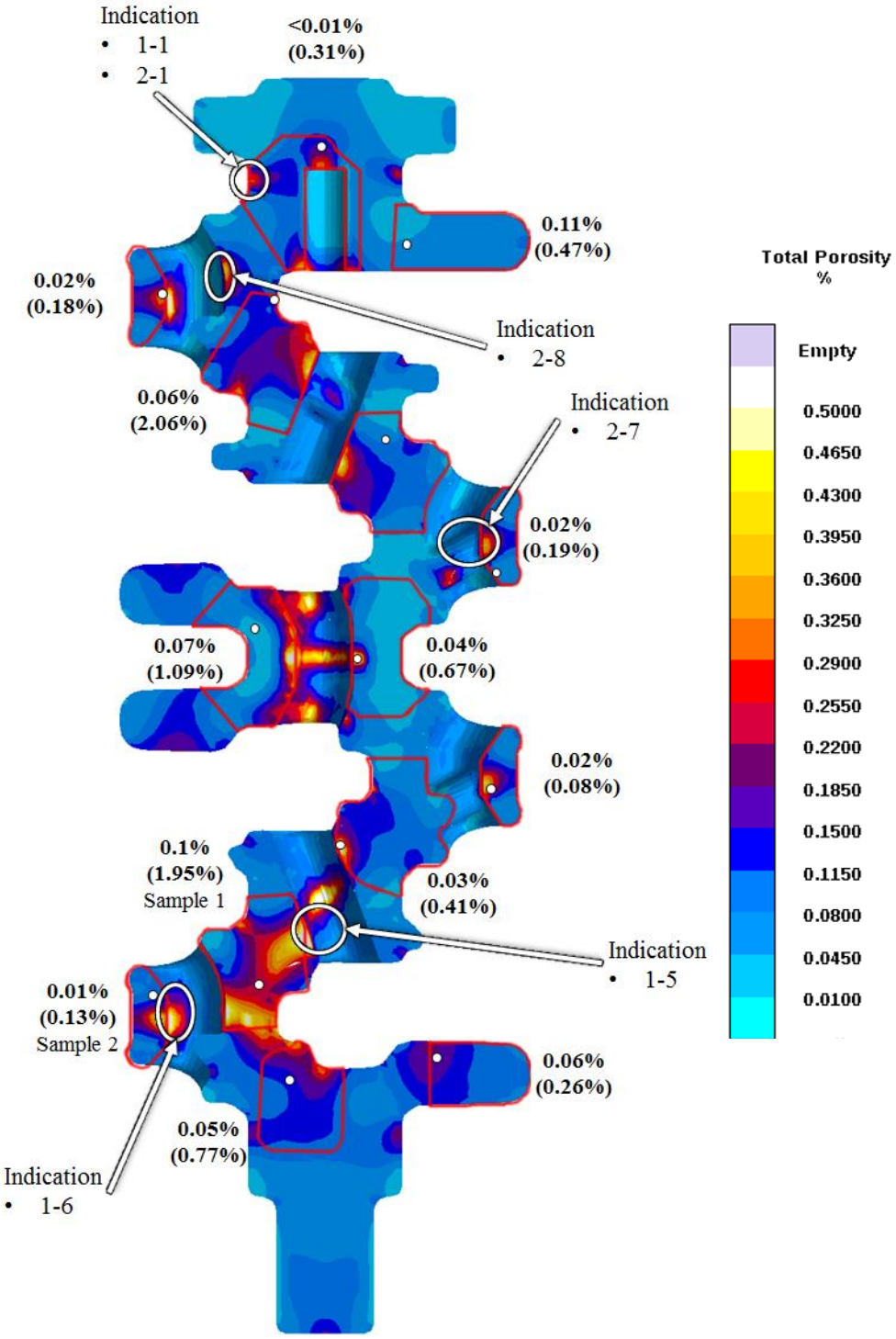

Figure 4.14 Contour of predicted microporosity overlaid with indications from the x-ray image that correlated to higher levels of predicted microporosity. The areas outlined in red represent polished sections cut from one of the crankshafts. The reported porosity, and max porosity in parenthesis, are adjacent to their respective polished section. White dots represent the location of the reported maximum porosity.

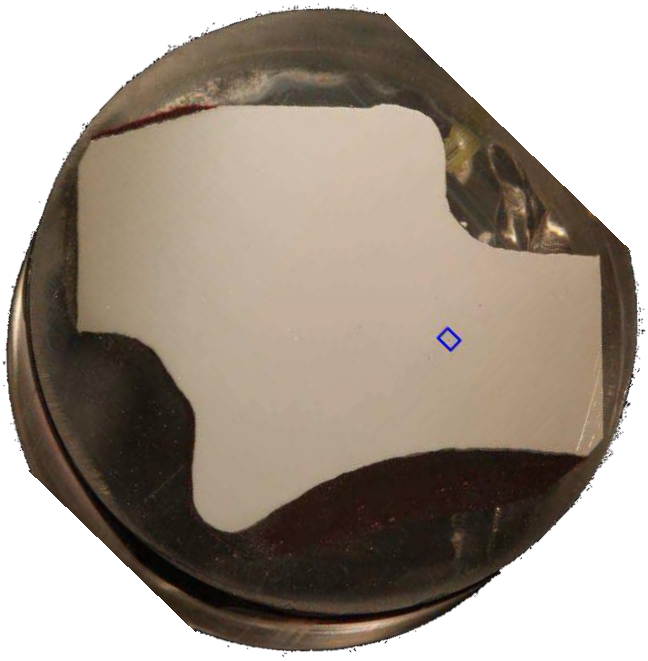

(a)

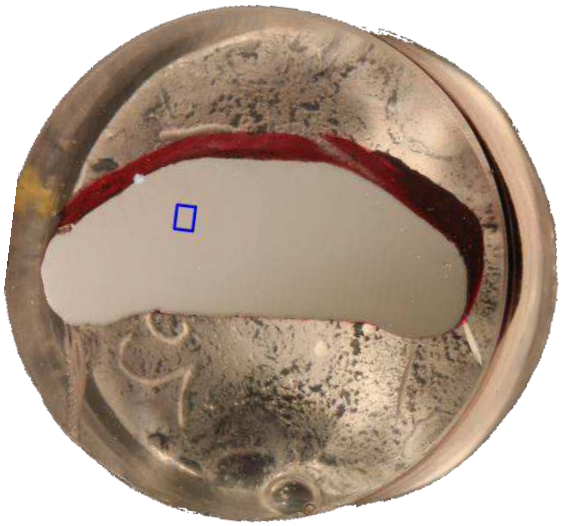

(b)

Figure 4.15 Photographs of polished (a) Sample 1 and (b) Sample 2. Each was cut from Crankshaft 1. The approximate location of maximum porosity is shown as a blue square in (a) and (b).

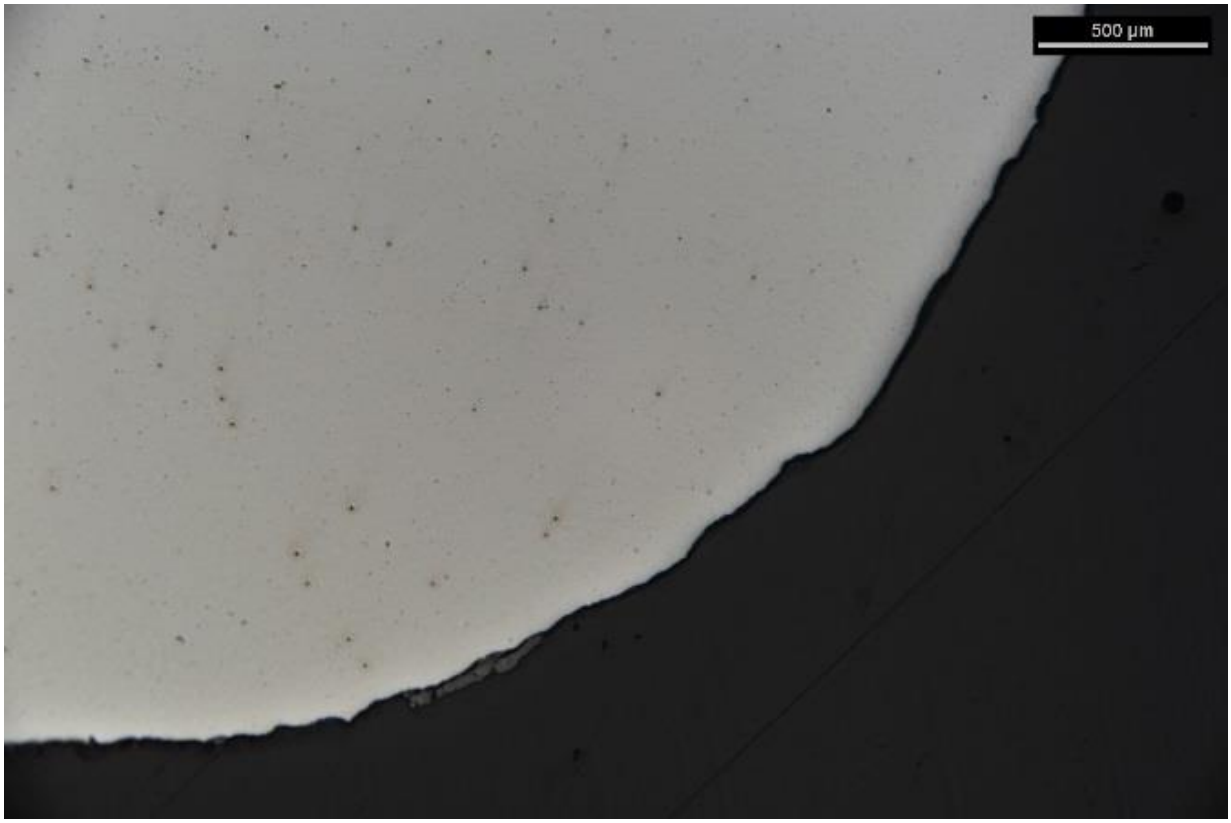

Figure 4.16 Example of one of the many photomicrographs from Sample 1. Magnification: 4x.

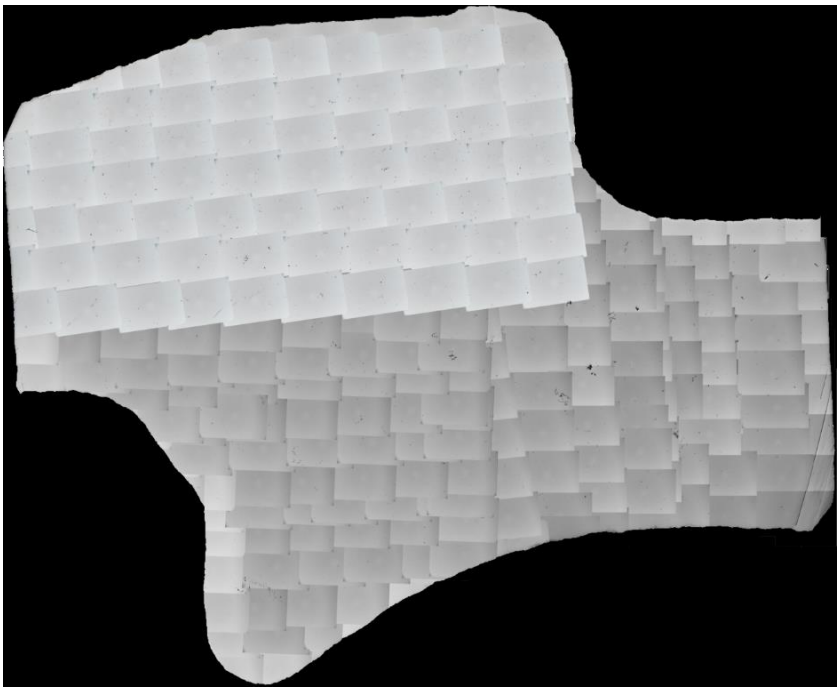

(a)

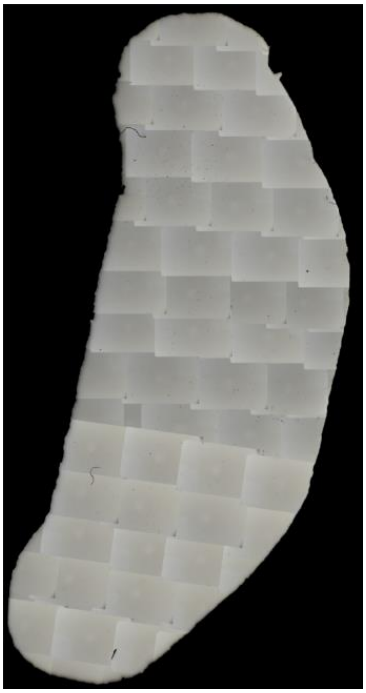

(b)

Figure 4.17 Stitched together images taken with a petrographic microscope, from (a) Sample 1, and (b) Sample 2.

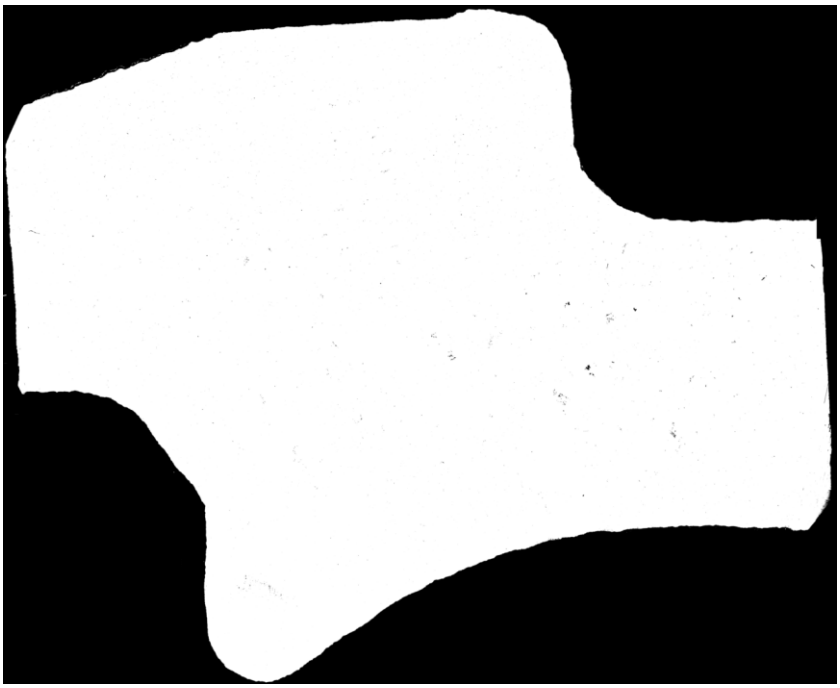

(a)

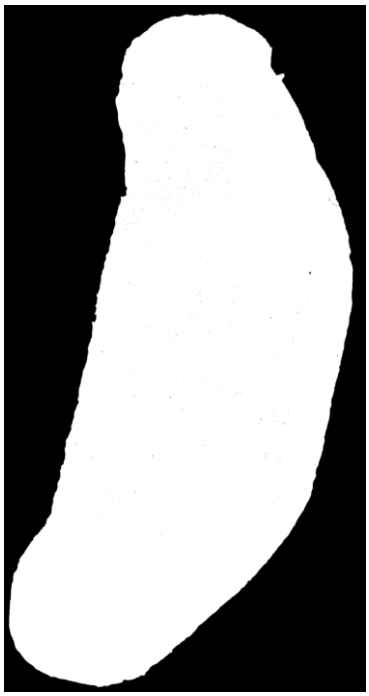

(b)

Figure 4.18 Binary images of (a) Sample 1, and (b) Sample 2, that represent porosity as black pixels.

Table 4.2 Percentage porosity comparison between results reported by Element Materials and calculated from the binary images of Sample 1 and Sample 2.

	Element Material Technology		Binary Images
Sample ID	% Porosity	Max Field %	% Porosity
1	0.1	1.95	0.09
2	0.01	0.13	0.06

(a)

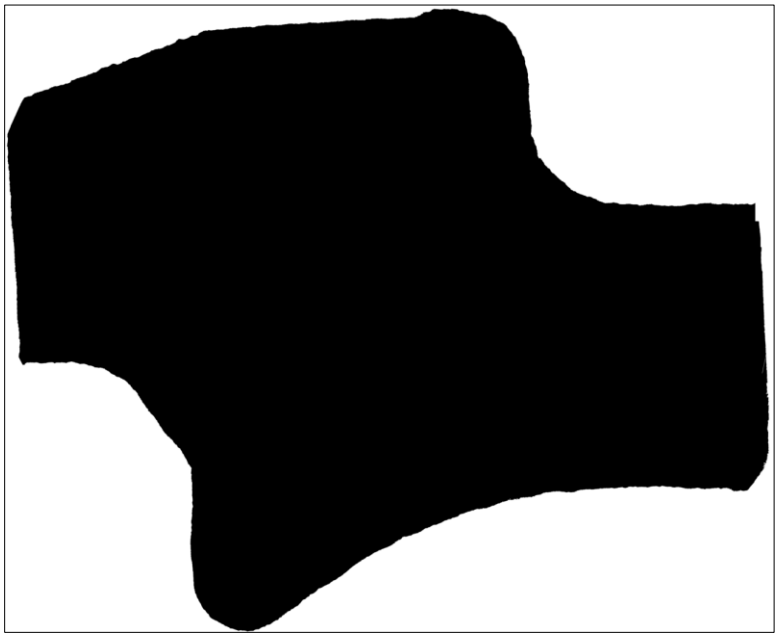

(b)

Figure 4.19 Deconstructed binary images of Sample 1. (a) Binary image without background and (b) Mask image.

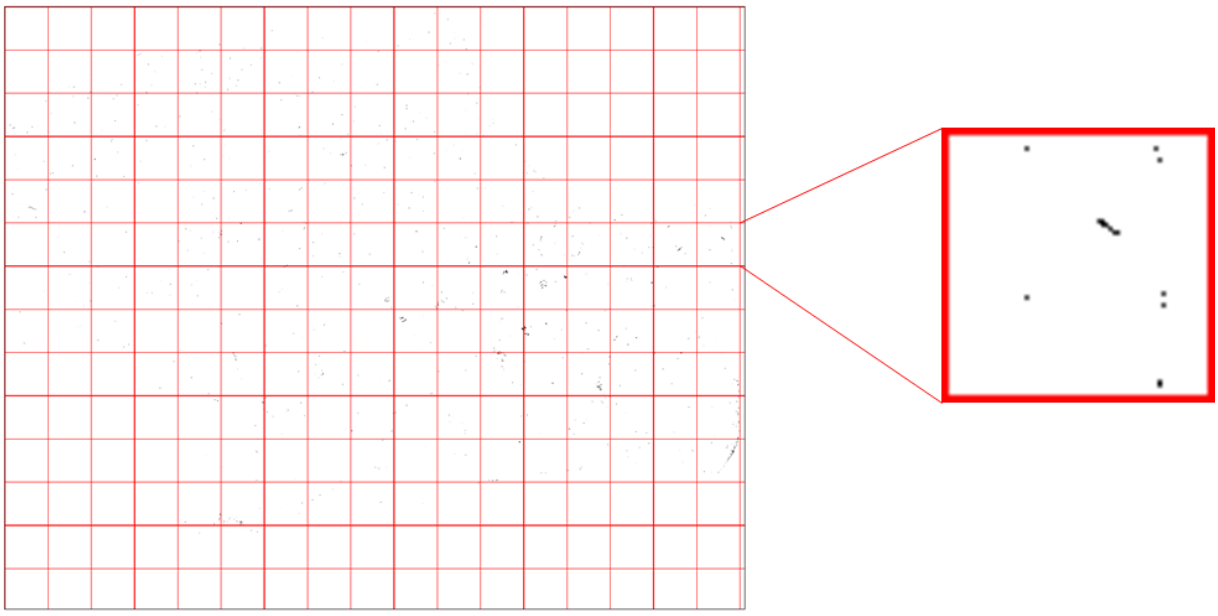

(a)

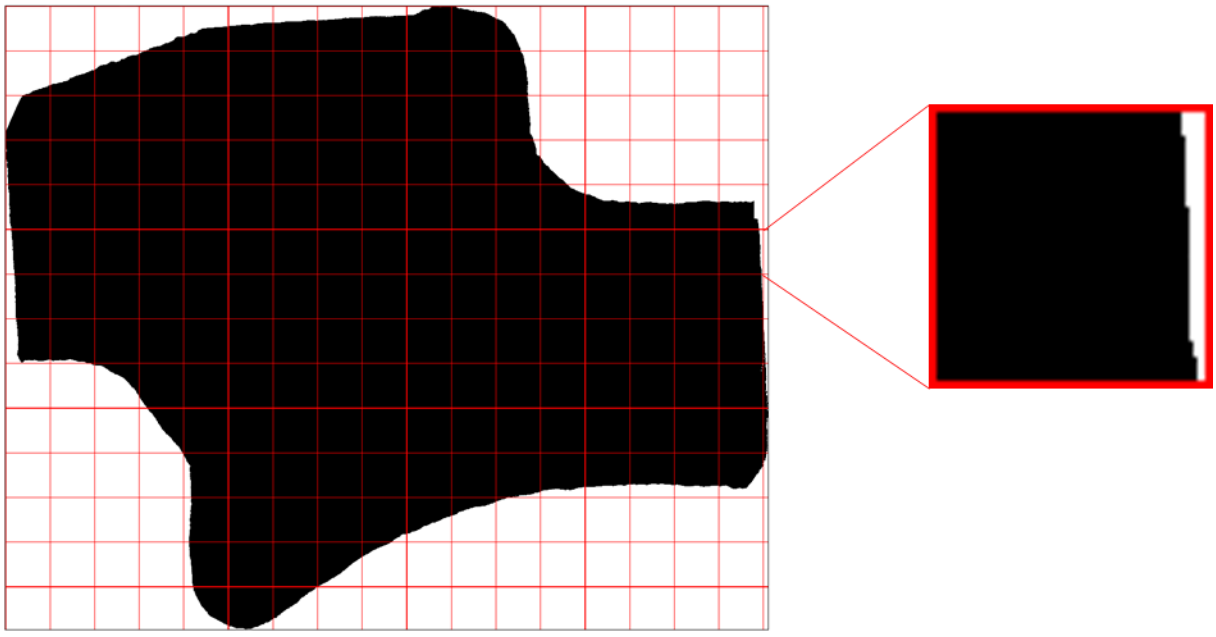

(b)

Figure 4.20 (a) Binary image without background and (b) Mask image broken down into a 600 by 600 pixel grid, with a magnified grid space.

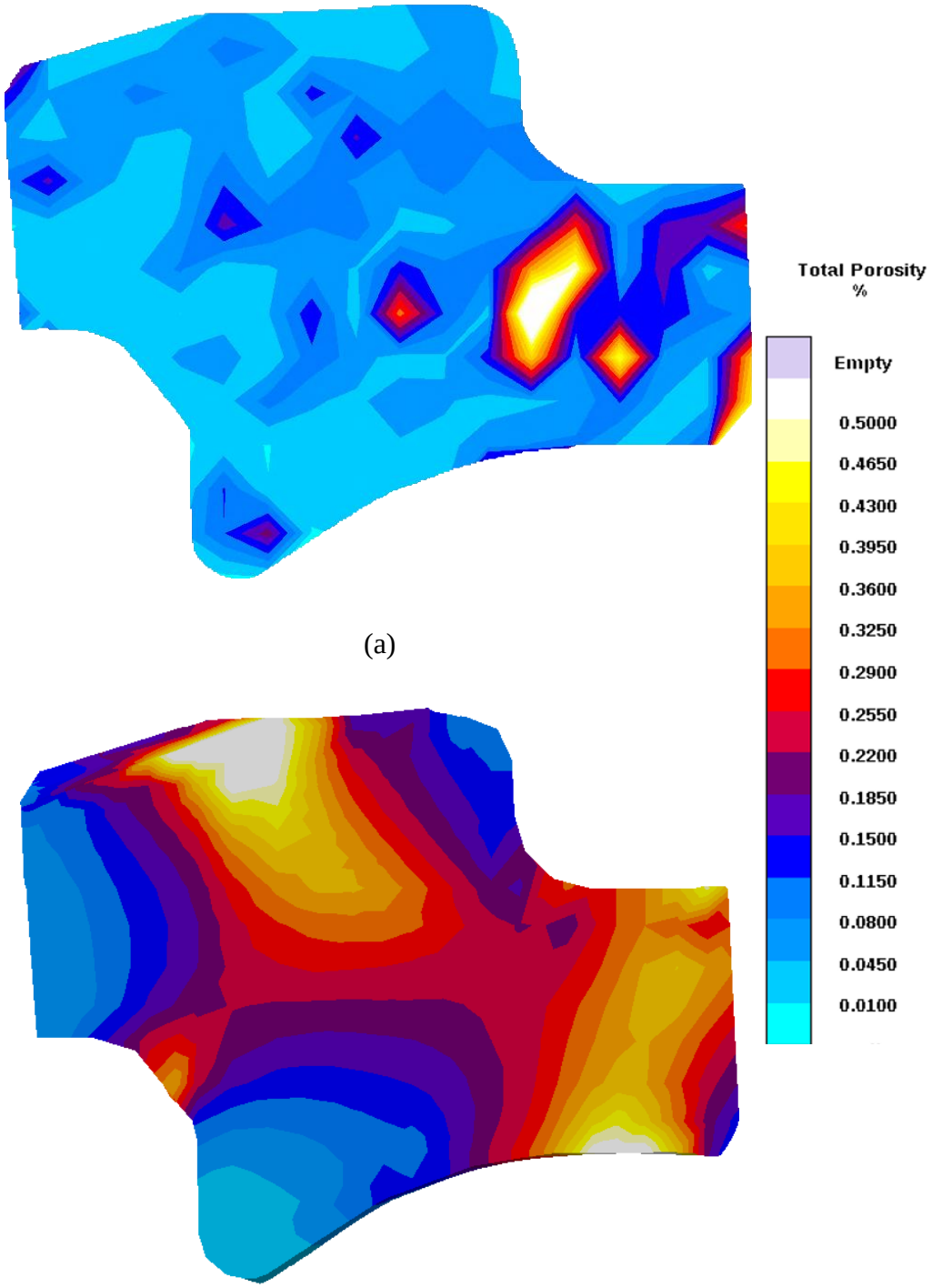

(a)

(b)

Figure 4.21 Percent porosity contours of Sample 1 (a) generated from the polished crankshaft sample and (b) from *MAGMAsoft*'s prediction of the same crankshaft.

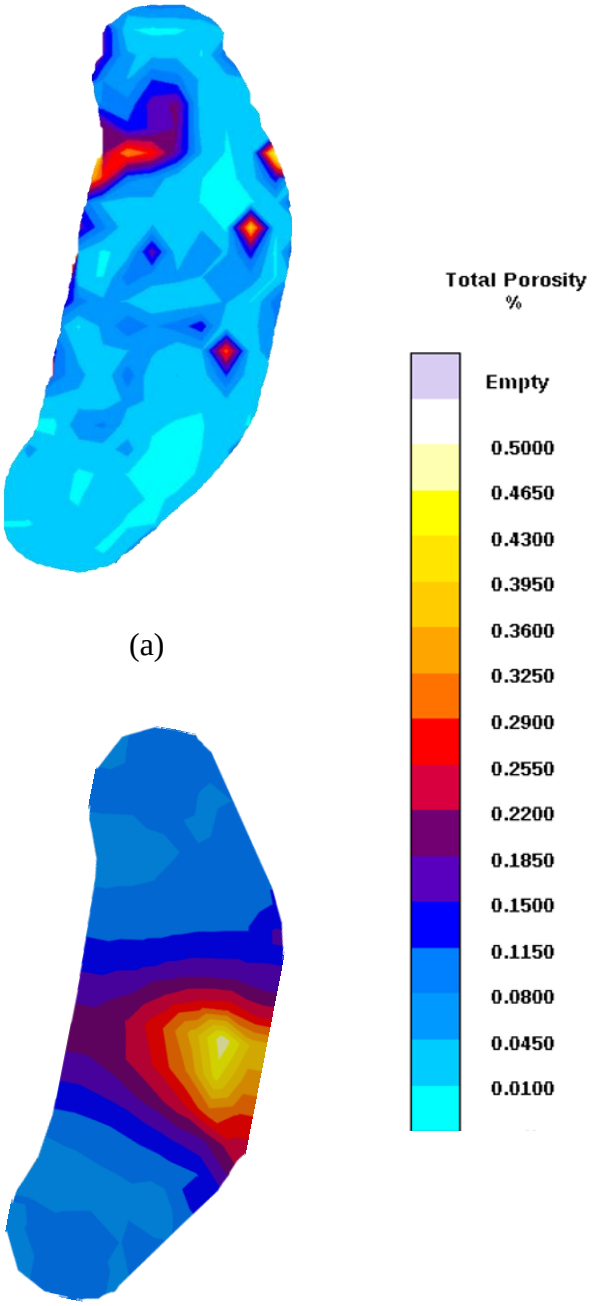

(a)

(b)

Figure 4.22 Percent porosity contours of Sample 2 (a) generated from the polished crankshaft sample and (b) from *MAGMAsoft*'s prediction of the same crankshaft.

CHAPTER 5: CONTINUED DELEOPEMENT OF CAST STEEL CRANKSHAFT RIGGING

5.1 Introduction

The gating system used in the previous chapters was prone to waterfalls and splashing during filling. This, along with the analyses performed in Chapter 6, prompted a revaluation of the rigging system for the cast steel crankshaft. Several changes were made to the rigging system. The most prevalent change was to the gating system. In order to promote a smooth and quiescent flow during filling, the crankshaft was gated into from every low point. A two-on rigging system was developed around this new gating system.

While, bottom gating through all of the low points of the crankshaft improved the filling. The initial drop of the metal down the sprue leads to reoxidation of the metal and can cause inclusions from the mold to be picked up. Counter-gravity filling avoids these casting defects. A single-throw (one-third) crankshaft rigging system was developed to be tested with the CFPS.

5.2 Two-on Cast Steel Crankshaft

Starting with the rigging used for the prototype crankshaft, several changes were made to the rigging based on the analysis of the x-ray images and previous simulation work. It was apparent that the risers located on the pin journals in the center of the crankshaft were not completely feeding the part. The diameter and neck thickness of the pin journal risers were increased. Simulations showed the increase in riser size reduced the levels of porosity beneath the pin journals in the part.

A new chill was added to the second main riser. Both the simulations and porosity reported by EMT showed relatively high levels of microporosity in the web between the first pin and second main journal. This area was deemed a critical area; therefore, the high levels of porosity present

were not tolerable. The new chill reduced the simulated porosity to more acceptable levels. The chill wrapped one quarter-way around the journal, and can be manufactured by a water-jet cutter.

The core located within the flange journal was removed after it was determined that during post-casting machining a hole would be drilled into the journal where the core was located, which rendered any porosity that forms in that location irrelevant. After the changes were made to the original rigging, development started on the two-on runner system.

Prototype crankshafts were filled with one gate beneath the riser in front of the crankshaft. Due to the shape of the crankshaft this method of gating is contributes to splashing and waterfalls while filling. This can lead to mold wall erosion and inclusions in the casting. A new gating system was developed the cast steel crankshaft. This gating system gated into every low point on the crankshaft. With nine in-gates into the casting, splashing and waterfalls, within the crankshaft, were eliminated while filling. This multi-point gating system was incorporated into the two-on mold design. A sprue, filter, and runner for the two-on rigging were designed so that the gating systems filled smoothly without jetting or turbulence.

The geometry of the two-on crankshaft rigging shown in Figure 5.1 was finalized, and simulations of filling and solidification were performed. After several iterations to the gating system, each gate filled evenly, shown in Figure 5.2, before entering the crankshaft cavity. Porosity predictions showed that the modifications made to the original rigging improved porosity and that the new gating system did not create additional porosity, resulting in an overall sound casting, shown in Figure 5.3.

5.3 Single-throw Crankshaft for Counter-gravity with Pressurization during Solidification

A single-throw crankshaft is a representative portion of the full sized crankshaft. A full crankshaft would be too large to test with the CFPS system designed in Chapter 6, so a rigging system was developed for a single-throw version of the GM SGE crankshaft. The single-throw model shown in Figure 5.4 was developed by GM, and is comprised of two main journals, one pin journal, and a counterweight. The all the journals except the rear main journal are hollow.

In a similar fashion to the full sized crankshaft, one large riser was used in front of the rear main journal. However, simulations showed this riser alone was not sufficient to feed the entire crankshaft. Several additional riser configurations were attempted, but all failed to feed the porosity at the opposite end of the first riser. Different chills were tested at various locations on the single-throw crankshaft, and finally a large chill placed at the opposite end of the riser reduced the porosity in the crankshaft to suitable levels.

The single throw crankshaft was gated into from every low point to prevent splashing during filling. The inlet to the runner was placed off center of the crankshaft so that it would be centered in the mold. An additional chill was placed at the inlet of the runner. This chill accelerated solidification at the inlet, which allowed the vacuum pressure to be released sooner

With the single-throw rigging design shown in Figure 5.5, finalized, a mold could be created and cast using the CFPS system. Counter-gravity filling, shown in Figure 5.6, and solidification without pressurization were simulated using the rigging developed. The predicted porosity shown in Figure 5.7 was comparable to the porosity predicted by the full-sized crankshafts in Chapter 3.

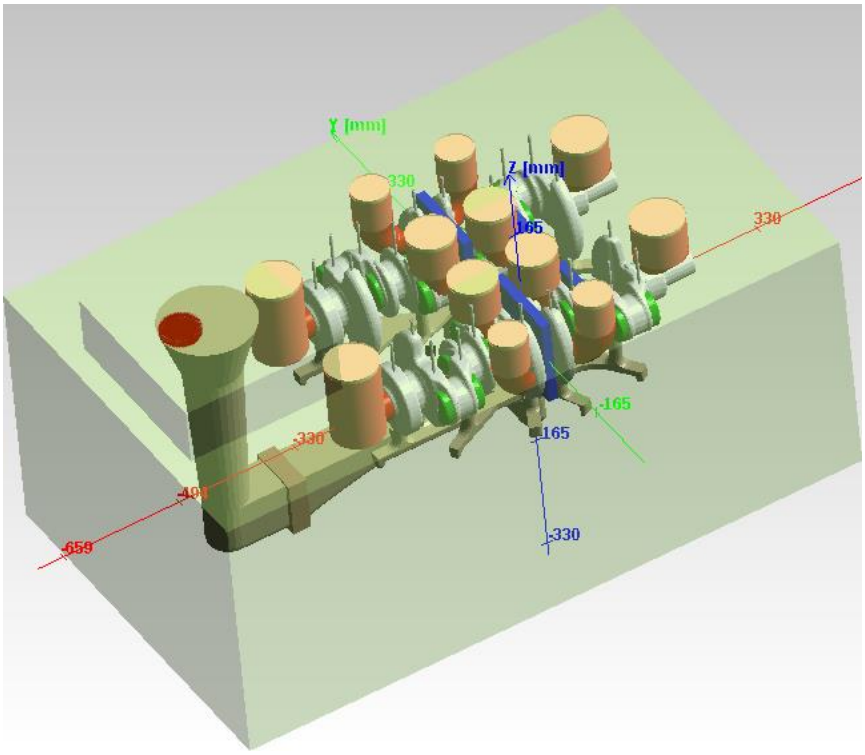

(a)

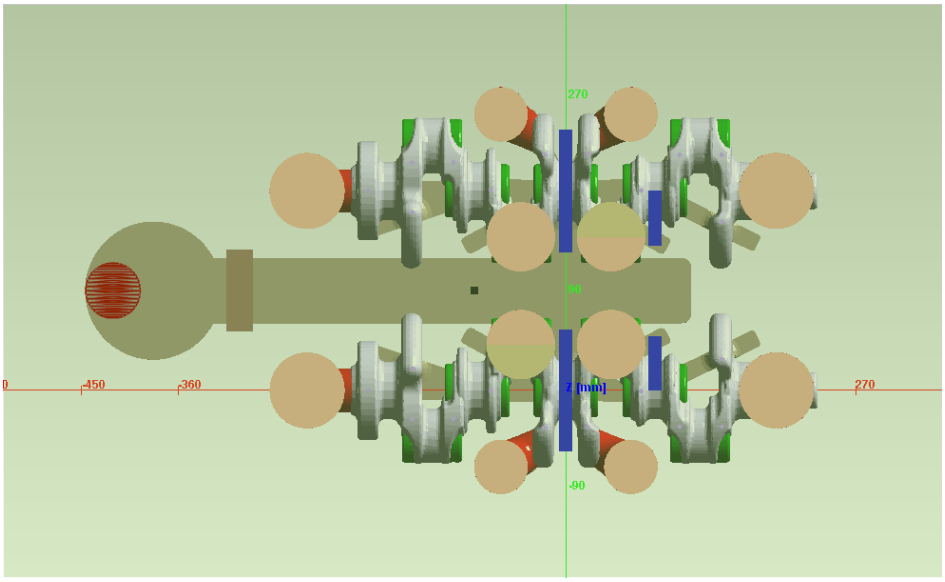

(b)

Figure 5.1 Two-on crankshaft rigging geometry. (a) Isometric view, (b) top view, (c) side view, and (d) bottom view.

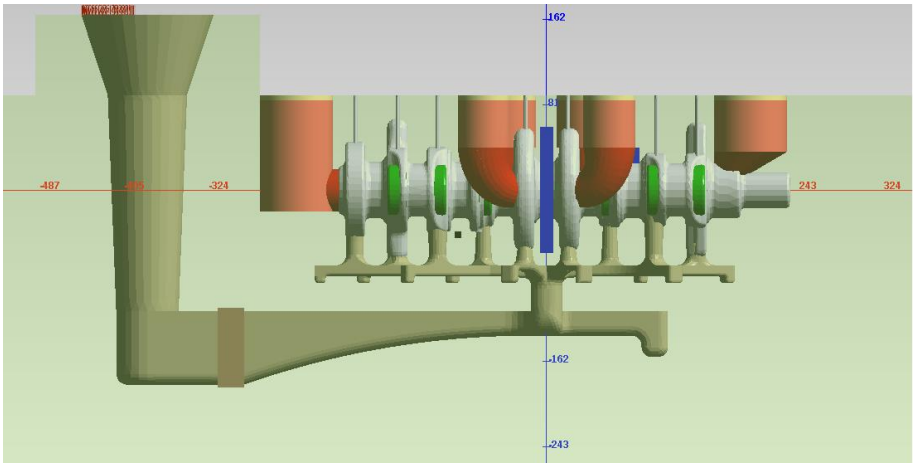

(c)

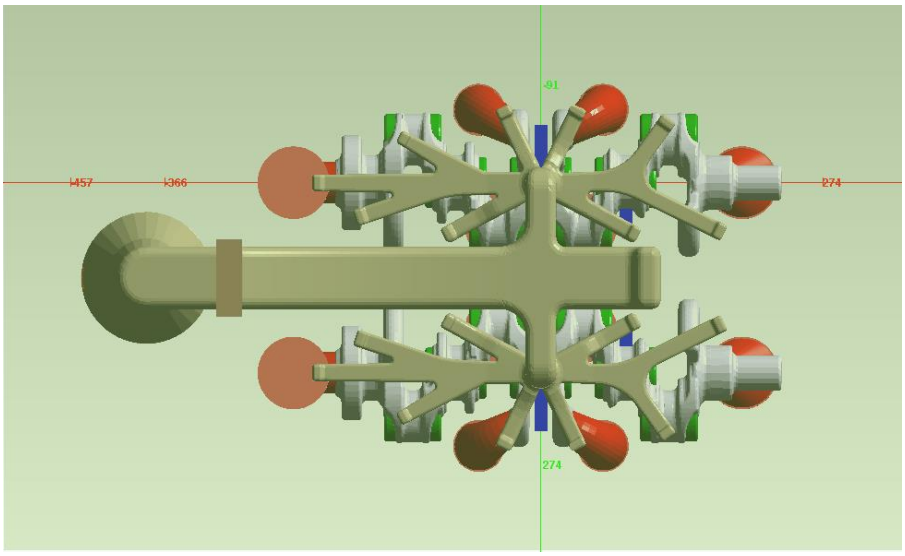

(d)

Figure 5.1 - continued

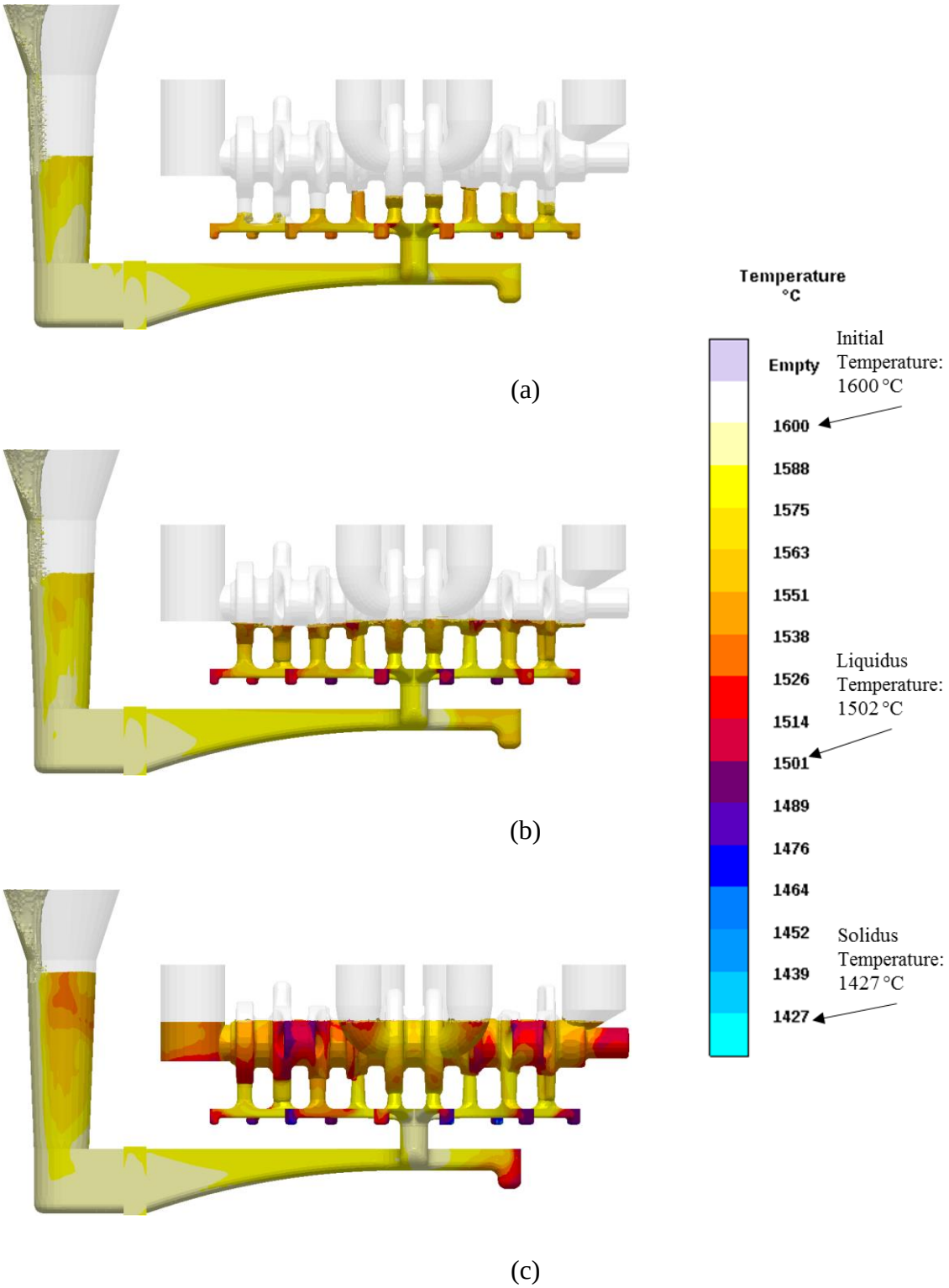

Figure 5.2 Two-on crankshaft mold filling simulation at (a) 4.0, (b) 5.0, and (c) 9.75 seconds.

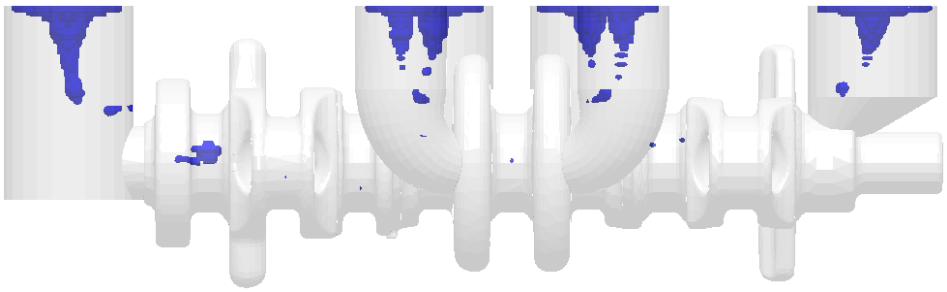

(a)

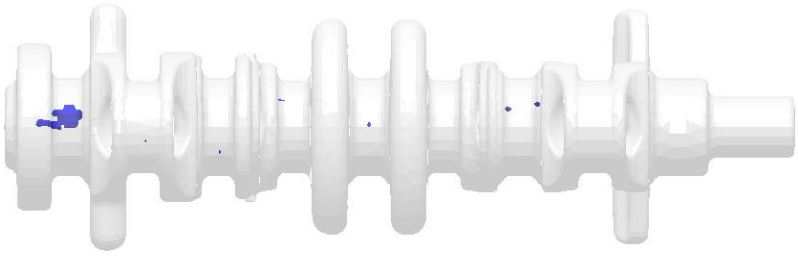

(b)

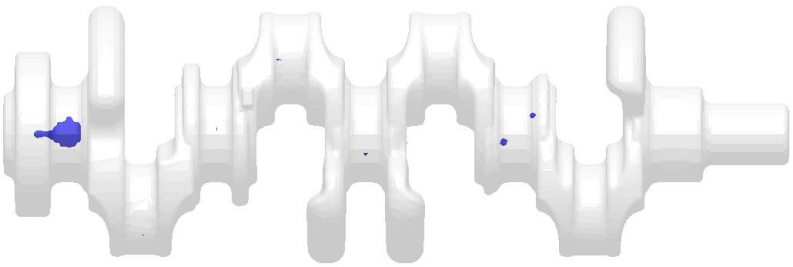

(c)

Figure 5.3 Two-on crankshaft porosity predictions. (a) Side view, (b) Side view with risers removed, and (c) top view with riser removed. Blue areas indicate predicted porosity within the crankshaft.

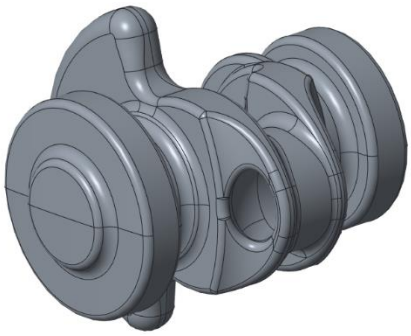

(a)

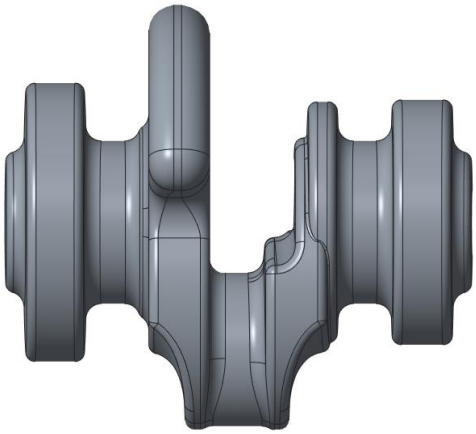

(b)

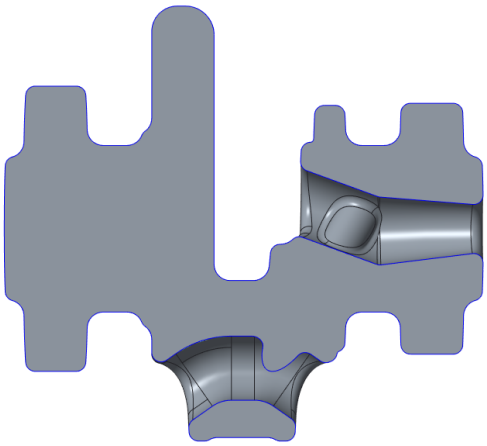

(c)

Figure 5.4 Single-throw crankshaft CAD model.

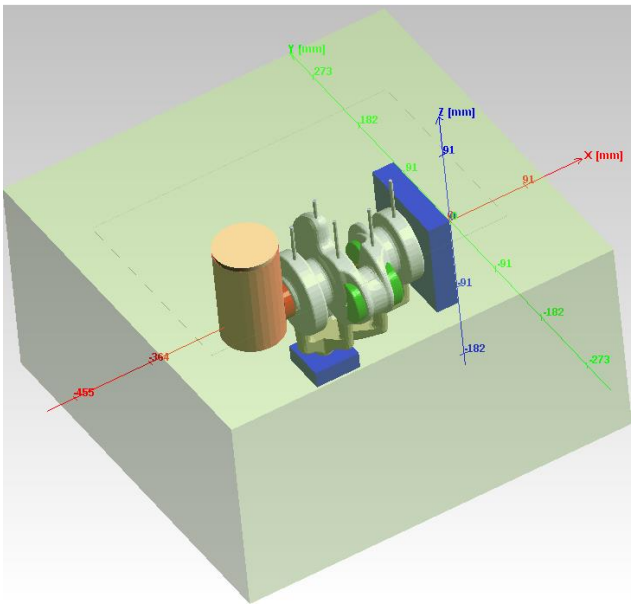

(a)

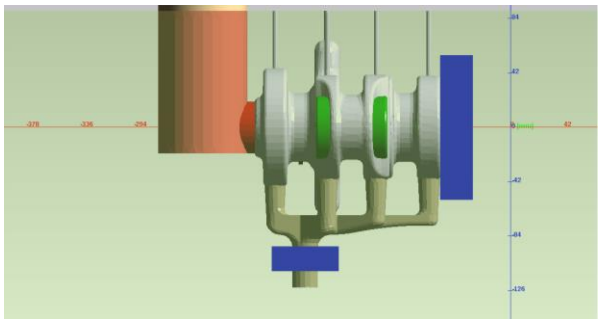

(b)

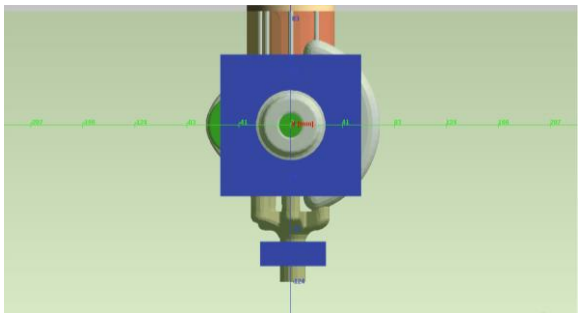

(c)

Figure 5.5 Final geometry for single-throw crankshaft CFPS rigging. (a) Isometric view, (b) side view, and (c) front view.

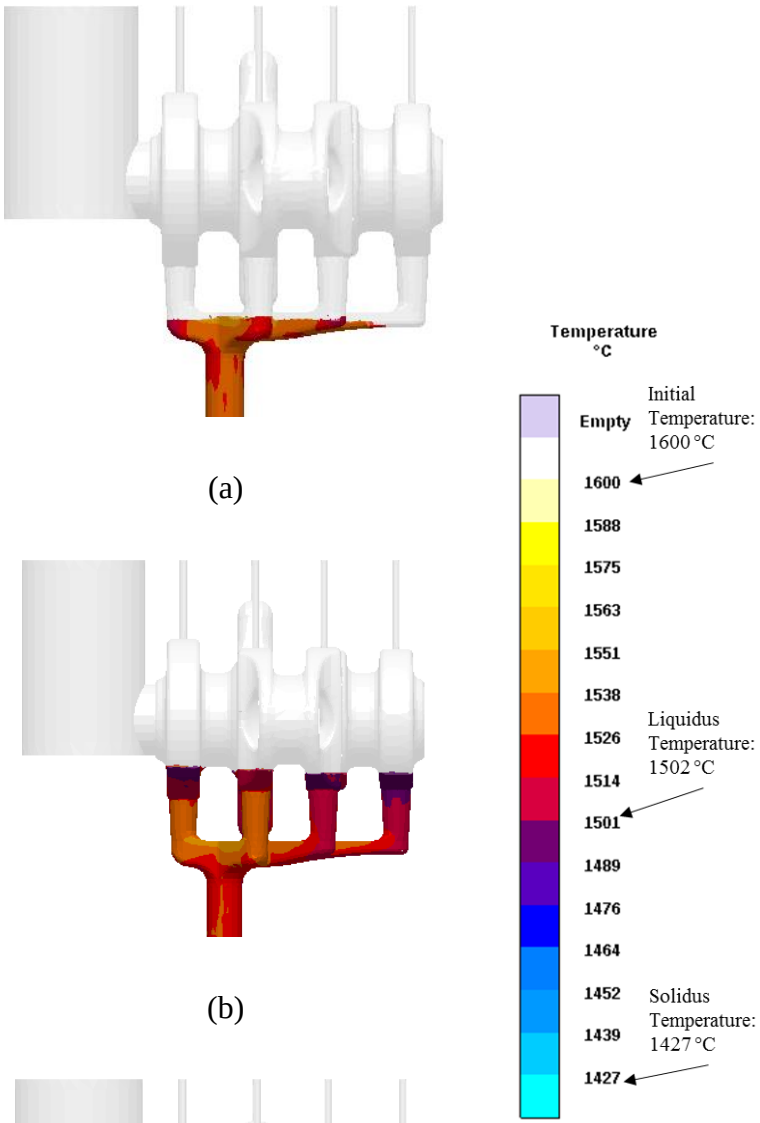

(a)

(b)

(c)

Figure 5.6 Simulated filling of the single-throw crankshaft mold, (a) Runner being filled, (b) liquid steel quiescently rises into the crankshaft cavity, and (c) Crankshaft filled smoothly other than a small waterfall into the riser.

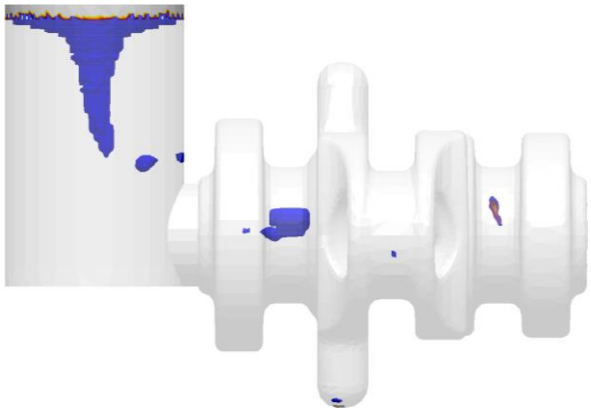

(a)

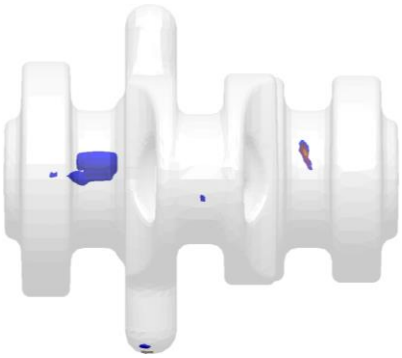

(b)

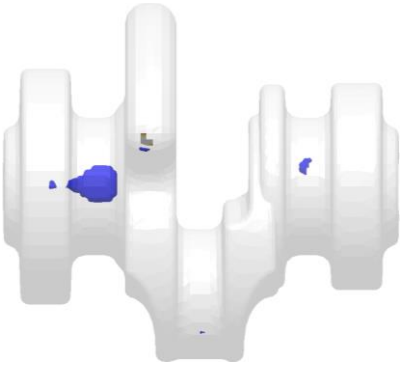

(c)

Figure 5.7 Single-throw crankshaft porosity predictions. (a) Side view, (b) Side view with riser removed, and (c) top view with riser removed. Blue areas indicate predicted porosity within the crankshaft.

CHAPTER 6: COUNTER-GRAVITY WITH PRESSURIZATION DURING SOLDIFICATION

6.1 Introduction

Both counter-gravity filling and pressurization during solidification have been found to improve casting properties. The casting will already be contained in an airtight chamber after it has been filled by the counter-gravity process. It is a straightforward process to pressurize the casting during solidification after a casting has been filled using counter-gravity. While both counter-gravity and pressurization during filling have been separately researched for steel alloys, any work related to the combination of the two process is scarce with steel alloys. A process was developed that utilizes counter-gravity filling and pressurization during solidification for steel alloys. Several experiments were performed to test the process. Gravity-filled control castings with pressurization were created, to compare with castings made by the CFPS process. All casting experiments were conducted at UNIMCC.

6.2 Process Design

The CFPS process is as follows: first, a sand mold is placed into an airtight vacuum chamber and the remaining space in the chamber is filled with loose sand. The entire chamber is raised above an induction furnace filled with molten steel. A fused silica ceramic snout protrudes from the bottom of the chamber, and is lowered directly into the molten steel. The pressure within the chamber is decreased steadily to 7.3 psia, which draws the liquid steel up the snout and into the mold cavity. An accumulator tank is used to "store" vacuum pressure because the vacuum pump alone would not reduce the pressure in the chamber before the liquid steel began to cool. A regulator is used to hold the pressure at a predetermined level, this keeps the mold full until the inlet below the mold solidifies, with the assistance of a chill. Once the inlet has solidified, the

vacuum pressure is released and the liquid steel remaining in the snout returns to the furnace. The vacuum chamber is moved on to a second chamber, named the pressure chamber, and the two chambers are sealed together. When the centerline of the casting has become 50% solidified, the entire system is pressurized to a maximum of 75 psia with nitrogen gas. Exothermic hot topping placed at the top of the riser prior to filling, keeps the metal at the top of casting's riser liquid while the rest of the casting forms a shell. The pressure then only acts on the top of the riser forcing the still liquid metal further into the casting. The system remains under pressure until the casting is fully solidified. The diagram in Figure 6.1 shows the components used during vacuum filling, in Figure 6.1 (a), and pressurization, in Figure 6.1 (b)

The entire system, shown in Figure 6.2, was first created in *CREO Parametric 2.0*, and then constructed in-house. The casting tested was a simple 2.5" diameter by 13" tall cylindrical bar with a riser above. The shape of the casting was chosen because simulation showed that without pressurization centerline porosity would be present. The mold, shown in Figure 6.3, included vents to prevent mold gas from affecting the casting and a steel chill at the inlet, so that the vacuum could be released sooner. Counter-gravity filling was simulated, Figure 6.4, to ensure the mold filled without the liquid jetting through the inlet. *MAGMAsoft* currently is not able to simulated pressurization during solidification, so solidification without pressurization was simulated to determine the time it took for the inlet to freeze (30 seconds) and the centerline of the bar to reach a solid fraction of 0.5 (roughly 200 seconds), which are shown in Figure 6.5.

In order to verify the effects of the CFPS process a traditional gravity-filled casting was developed. The casting included the same bar as the CFPS mold, however a runner and sprue were the means for the liquid metal to enter the bar. The runner system of the control castings was designed so that the bar filled as smoothly as possible for a gravity-filled casting,

6.3 Experiments and Results

Two trials of the CFPS process were conducted with moderate success. During the first trial, one CFPS mold was cast in WCB steel, a low-alloy steel. The mold was filled in 8 seconds. However, the pressure set on the regulator was slightly higher than desired; this resulted in the bar's riser not being filled after the inlet had frozen off shown in Figure 6.6. After 30 seconds, the vacuum was released, and the chamber was transferred over to the second chamber and latched down. The entire system was pressurized; but due to a leak between the two chambers, the maximum pressure reached was only 36 psia. The pressure was maintained for 60 second after the casting had reached a solid fraction of 0.5. Figure 6.7 shows the pressure history throughout the experiment. X-rays later revealed that the pressurization had no effect on the porosity in the casting, and the CFPS casting from this trial produced a worse casting than the gravity-filled control cases because the riser of the CFPS casting did not fill. Two gravity-filled control molds were filled from the same heat, Figure 6.8 and Figure 6.9. While the riser did not fill completely the concept of the CFPS process was shown to be possible.

For the second trial, several changes were made to the system and process. First, the latch locks shown in Figure 6.2 were installed to the pressure chamber to improve the seal between the two chambers. Second, two three-way valves were added between the regulator and vacuum chamber, shown in Figure 6.1. These valves allowed for better control of pressure and a quicker release of pressure in the system. The height and diameter of the casting's riser was increased, so that if the riser was not filled completely there would still be sufficient liquid metal to be forced by the pressure into the casting. Simulation of the new riser showed that without pressure the centerline porosity present was nearly identical to the porosity simulated for the control castings. Following the same procedure as the previous experiment, the pressure was lowered in the vacuum

chamber to fill the mold. During filling, the pressure dropped slightly below the desired level, which caused some metal to flow over the top of the mold. However, the pressure was returned to the correct level before the inlet solidified. When the inlet had solidified the vacuum chamber was moved and latched down to the pressure chamber, and the entire system was pressurized after 220 seconds to a maximum pressure of 50.7 psia, due to some leakage, the pressure dropped and held steady at 43.5 psia, shown in Figure 6.10. The second trial was much more successful than the first. The riser was almost completely filled, Figure 6.11, and pressure was applied in adequate time. No control castings were cast during the second trial, and the same steel alloy was used.

Radiographs were taken of all the castings, Figure 6.12, from both trials to ascertain if the CFPS process was successful at feeding the centerline porosity. The first CFPS trial possessed significantly more porosity, because the casting had no riser. The radiograph of the second CFPS trial did not contain any visible centerline shrink that is present in both of the control castings.

The first gravity-filled casting and the second CFPS trial casting were cut through the vertical midplane. A dye penetrant test was performed on one-half of each cut casting, shown in Figure 6.13. The test showed that the CFPS casting possessed none of the centerline shrinkage that was present in the gravity-filled casting. Both the x-ray images and dye penetrant tests indicated that the CFPS process has the potential to eliminate centerline porosity that would otherwise be present in a gravity-filled casting. Additional trials would be needed to verify the effects of the CFPS process.

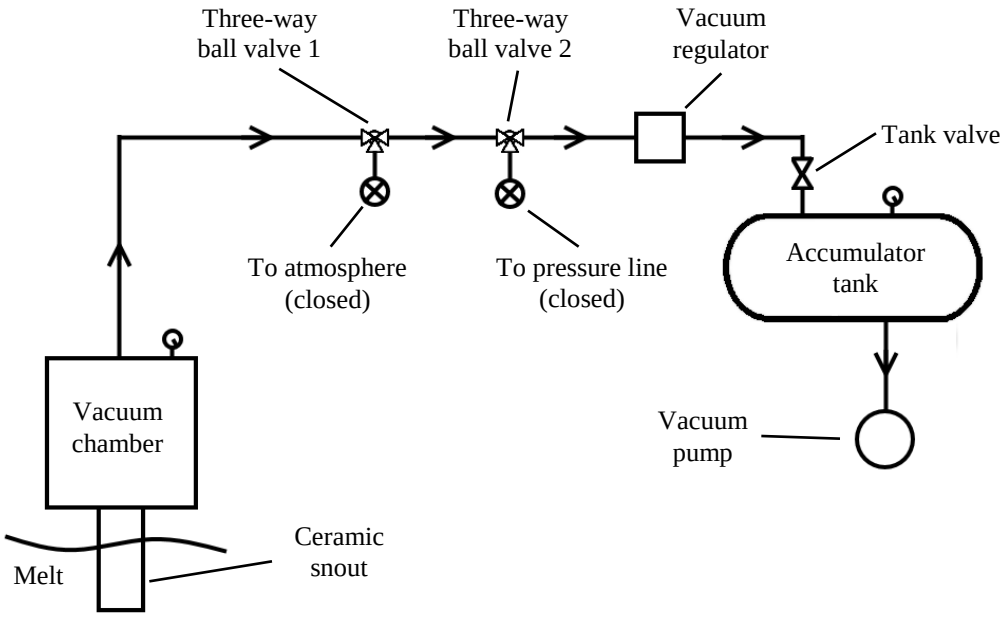

(a)

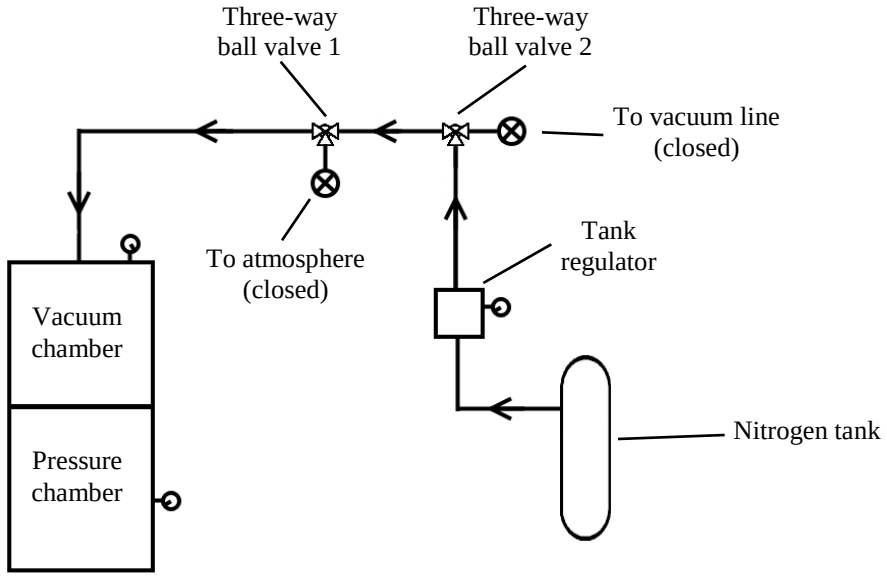

(b)

Figure 6.1 Diagram of the CFPS process, (a) during filling and (b) during pressurization. Arrows indicate the direction of airflow.

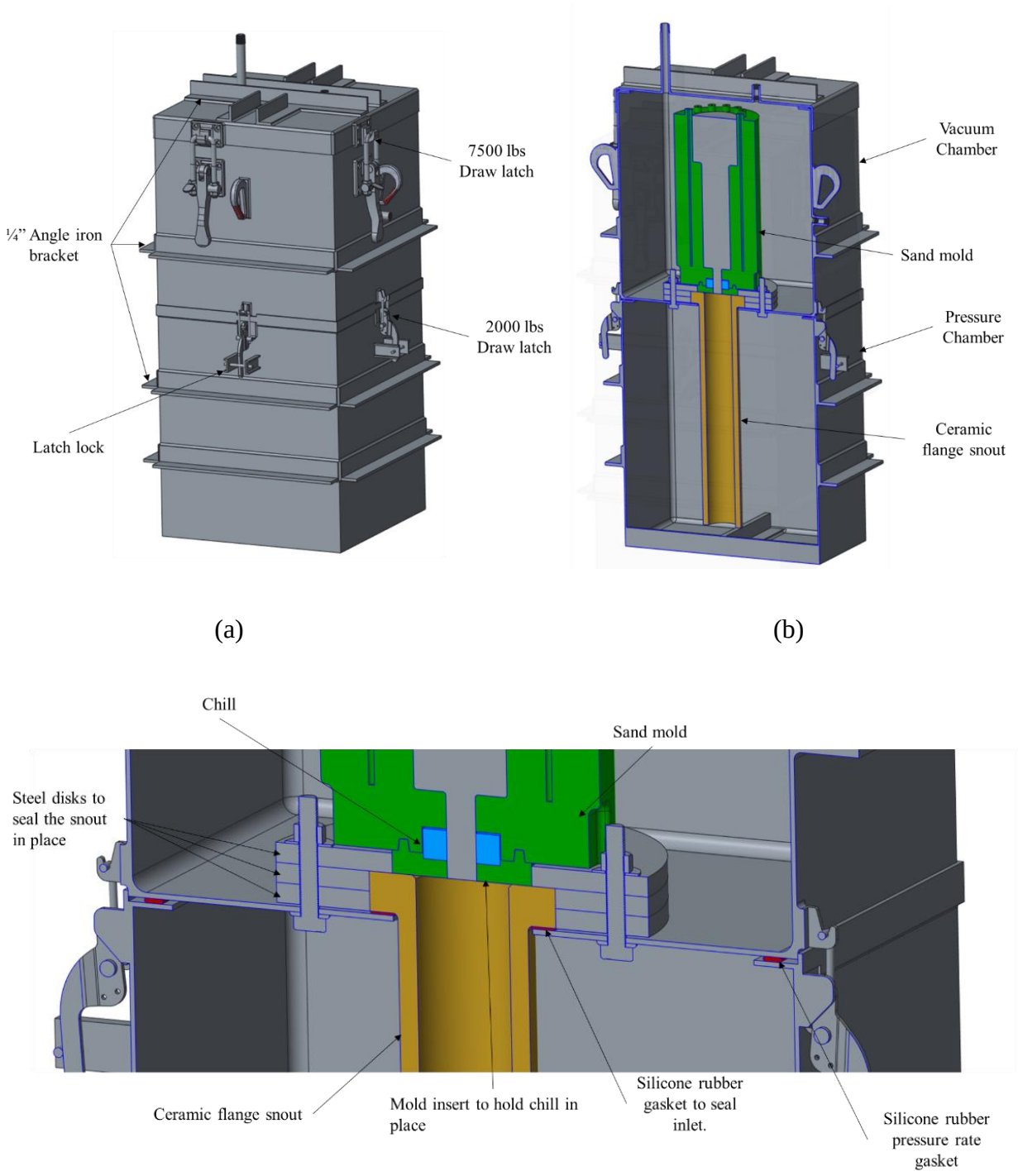

Figure 6.2 CFPS system. (a) Outside, (b) a cut through the vertical midplane, and (c) a close up of the connection between the vacuum and pressure chamber.

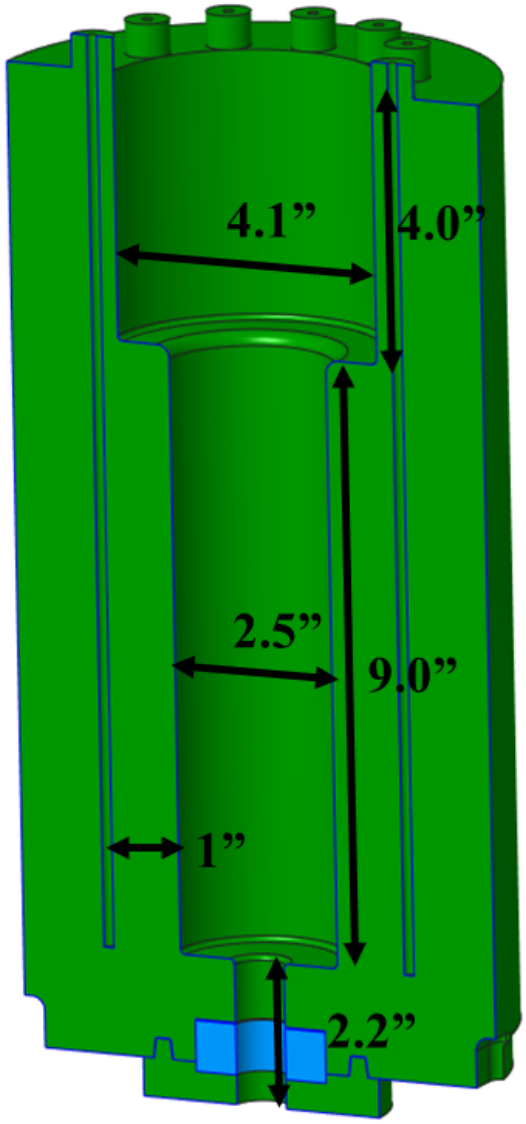

Figure 6.3 Mold used for the CFPS process cut through the vertical midplane.

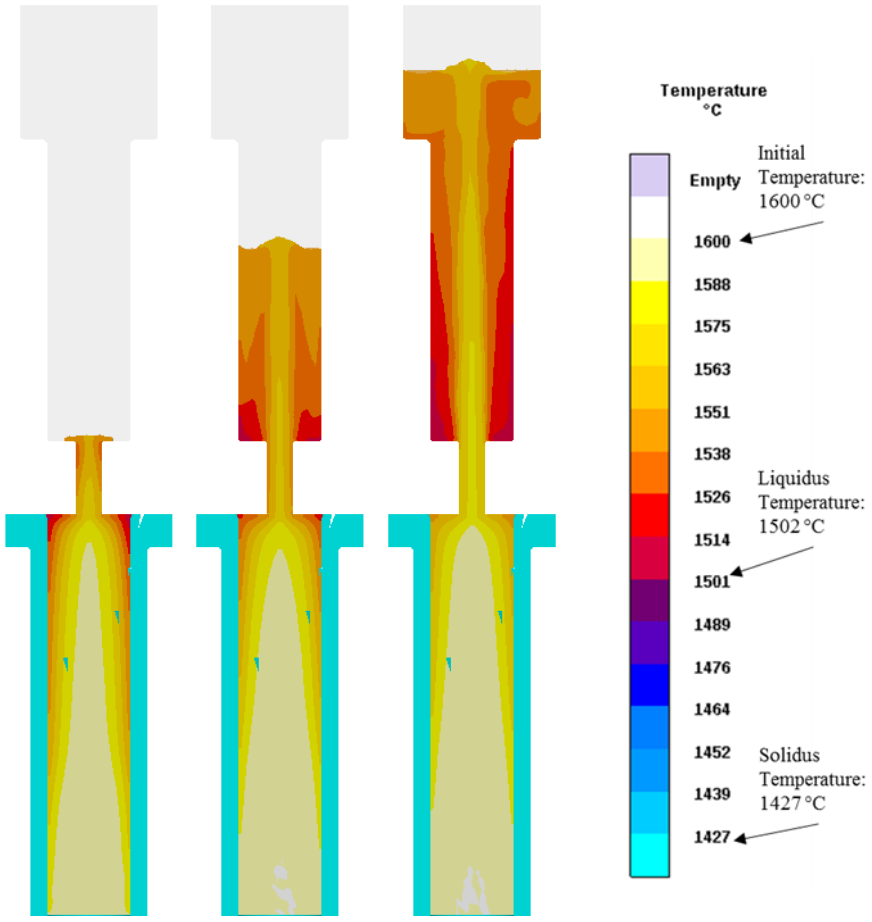

(a) (b) (c)

Figure 6.4 CFPS mold filling simulation at (a) 8.3, (b) 11.7, and (c) 17.7 seconds.

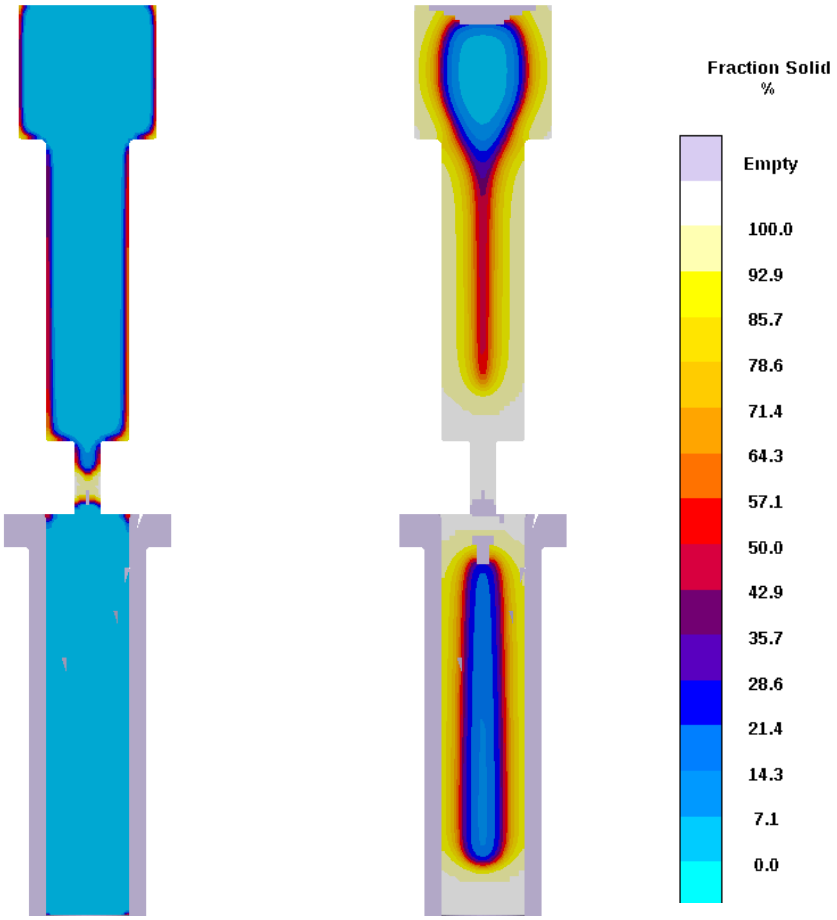

(a) (b)

Figure 6.5 Predicted contours of fraction solid during solidification. At (a) 36 seconds the inlet freezes off, and at (b) 220 seconds the centerline of the casting is 50% solid.

(a)

(b) (c)

Figure 6.6 Casting results of the first CFPS trial showing (a) the full casting, (b) the inlet, and (c) the unfilled riser.

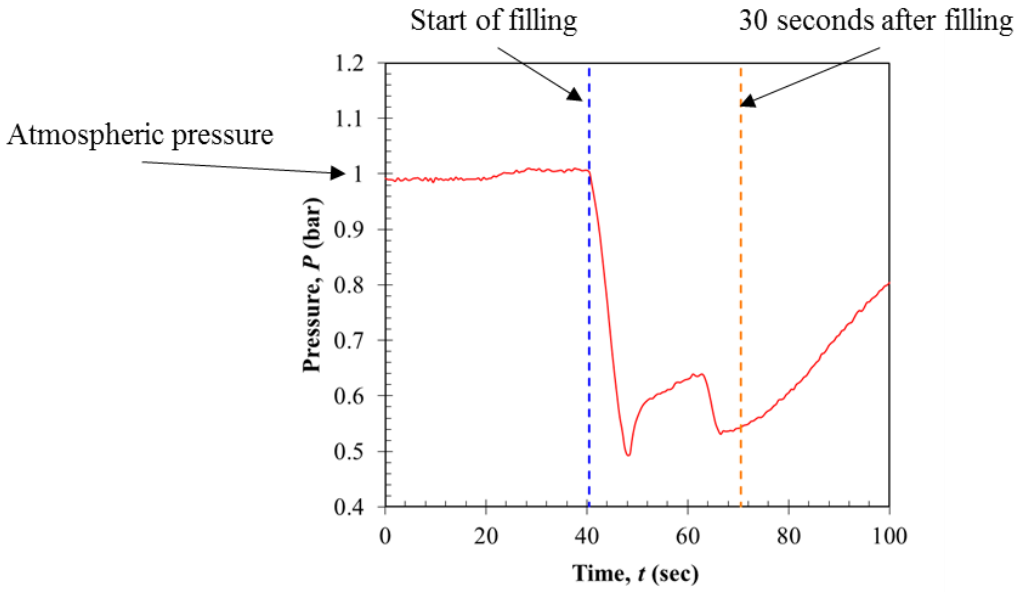

(a)

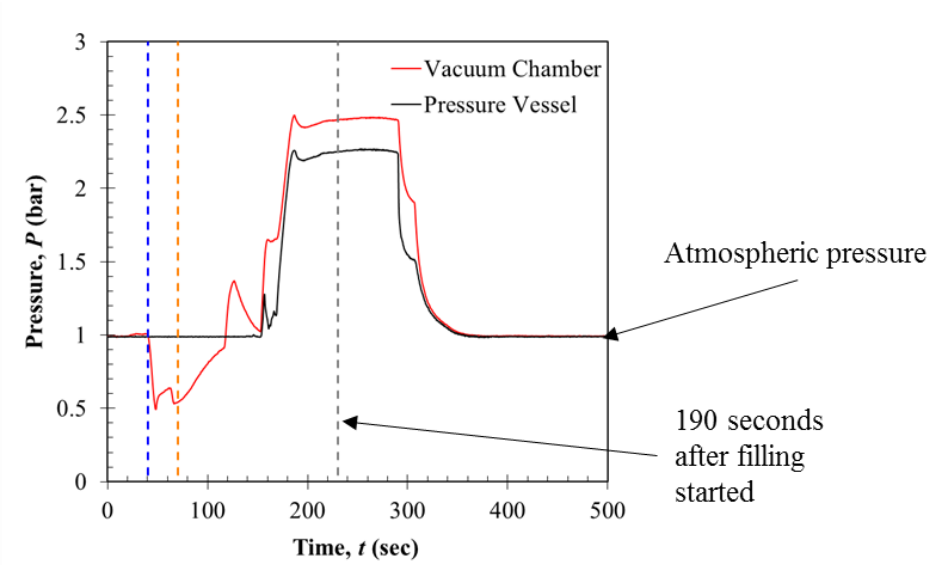

(b)

Figure 6.7 History of pressure within the vacuum and pressure chambers during (a) the initial pressure drop and filling of the mold and (b) the total pressure history of the first trial.

(a)

(b)

(c)

Figure 6.8 Casting results of the first gravity-filled mold showing, (a) the full casting, (b) a close up of the casting surface, and (c) the riser.

(a)

(b)

(c)

Figure 6.9 Casting results of the second gravity-filled mold showing, (a) the full casting, (b) a close up of the casting surface, and (c) the riser.

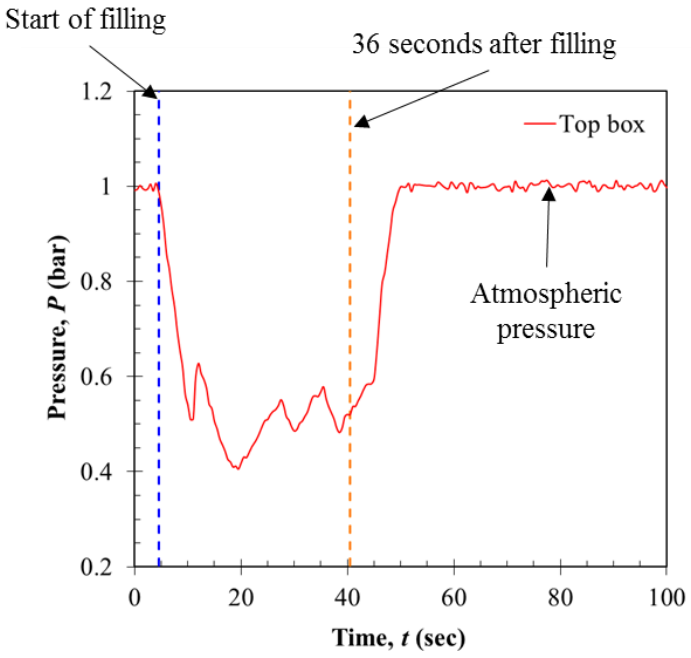

(a)

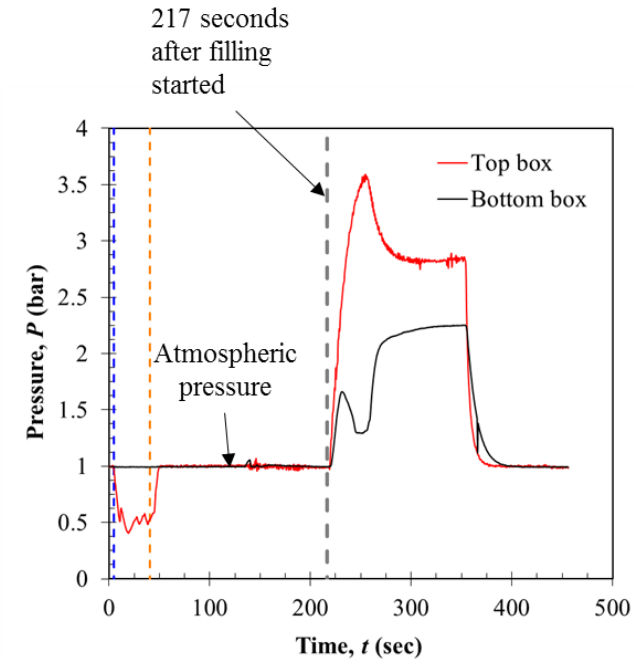

(b)

Figure 6.10 History of pressure within the vacuum and pressure chamber during (a) the initial pressure drop and filling of the mold and (b) the total pressure history of the experiment, of the second trial.

(a)

(b) (c)

Figure 6.11 Casting results of the first CFPS trial showing (a) the full casting, (b) the inlet, and (c) the riser.

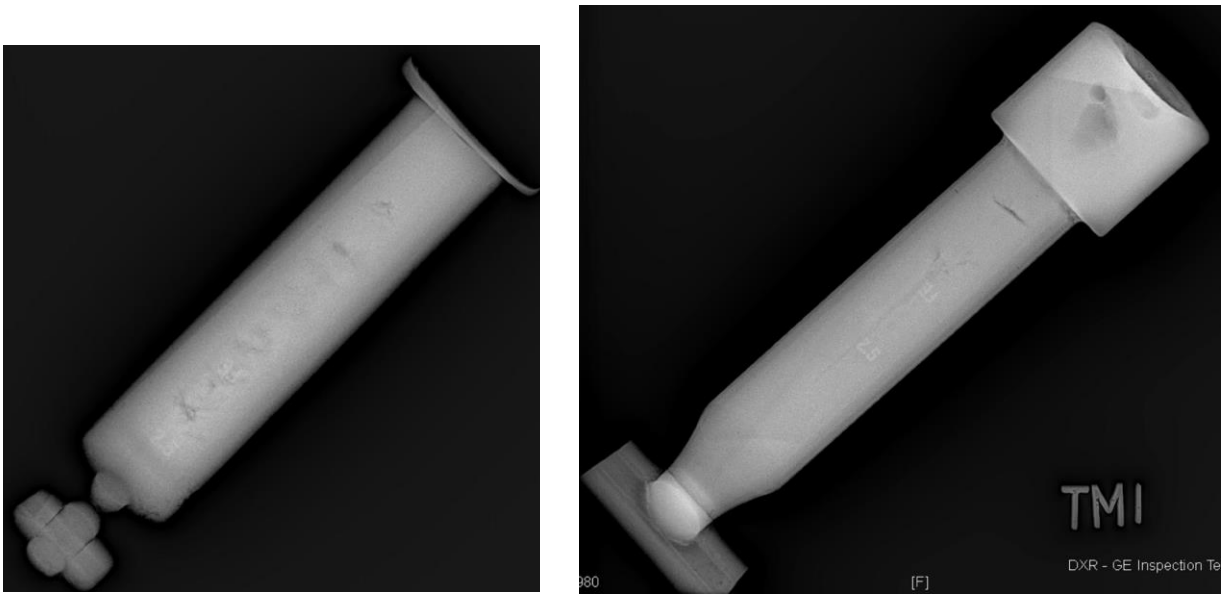

(a) (b)

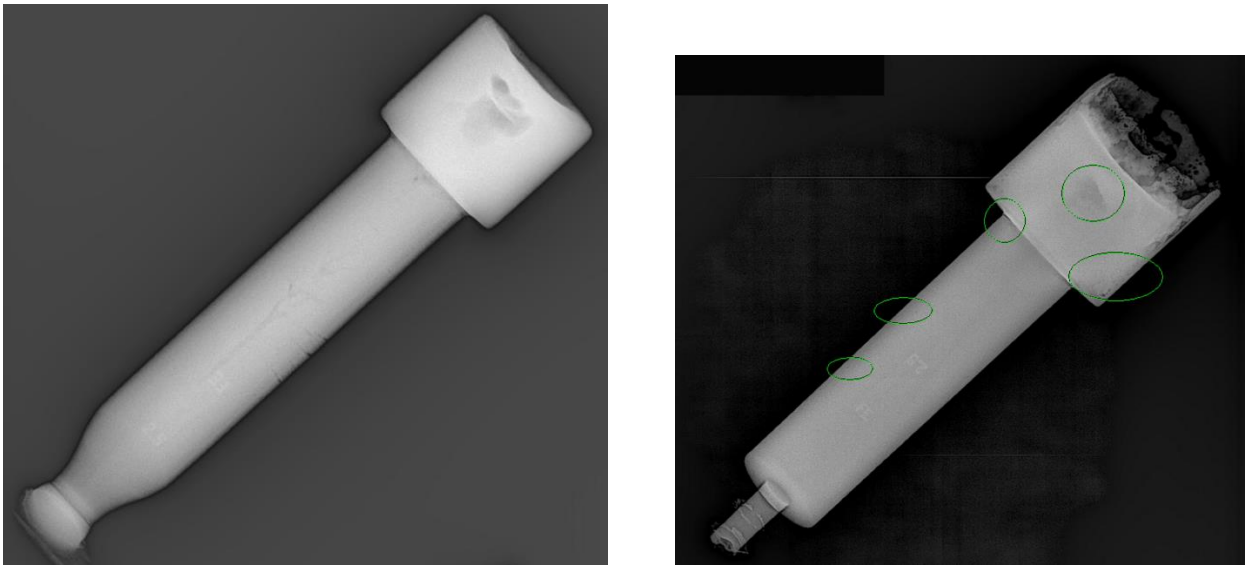

(a) (b)

Figure 6.12 X-ray images of the casting (a) from the first CFPS trial, (b) first gravity-filled mold, (c) second gravity-filled mold, and (d) the second CFPS trial.

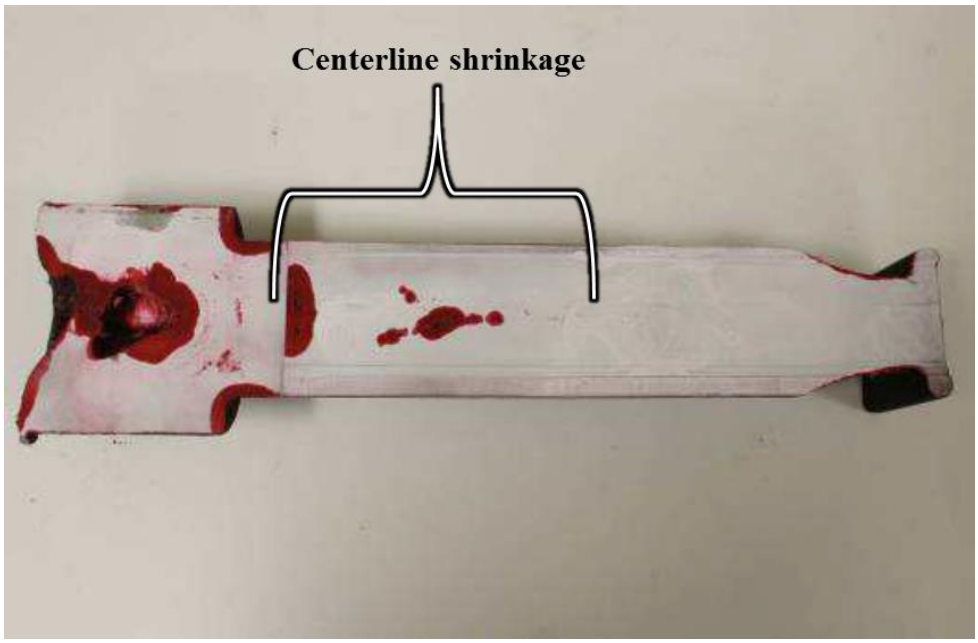

(a)

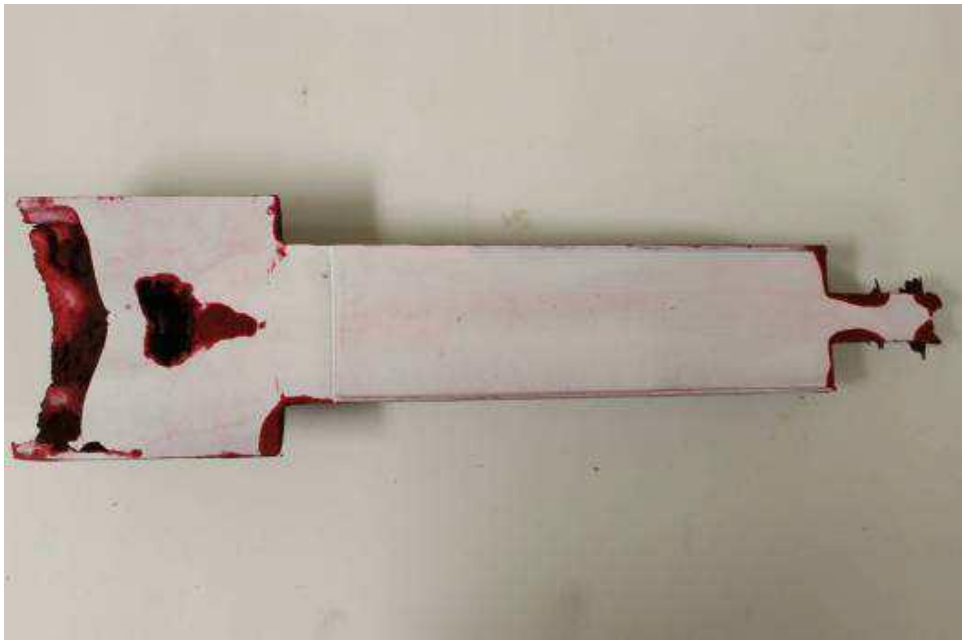

(b)

Figure 6.13 Dye penetrant test results from the (a) first gravity-filled mold and (b) the second CFPS trial.

CHAPTER 7: CONCLUSIONS AND RECOMMENDATIONS FOR FUTURE STUDIES

7.1 Conclusions

A riser and gating system was developed for a cast steel crankshaft, through an iterative risering process. The crankshaft rigging was simulated using *MAGMAsoft* and found to have low levels of predicted porosity. A CAD model of a sand mold was created for castings a steel crankshaft based on the rigging designed. Two sand molds were printed and two prototype cast steel crankshafts were cast. Analyses of the prototype crankshafts were in good agreement with predicted porosity. A few modifications to the crankshaft rigging system were made. The new rigging model was gated into every low point on the crankshaft, and featured two crankshafts per mold. In order to test the effects of the CFPS system, rigging and gating were designed for a single-throw crankshaft.

A new process for casting steel was developed by combining counter-gravity filling with pressurization during solidification. A CFPS system was designed and produced, using CAD modeling and casting simulations. Two CFPS trials were conducted. During the first trial the riser failed to fill, so the pressure was ineffective, however in the second attempt the riser was nearly filled completely. X-ray images and dye penetrant tests of the CFPS castings were compared to the gravity-filled castings. No centerline porosity is visible in the x-ray or dye penetrant of the second CFPS casting, in contrast gravity-filled castings in which the centerline porosity is very obvious.

7.2 Recommendations for Future Studies

Further testing of the CFPS process is needed to verify the results of the second CFPS trial. These tests could include a larger variety of casting shapes and sizes. A crankshaft would be an

excellent test casting for the CFPS system, the shapes of the journals and webs lead to many waterfalls and splashing during filling, which counter-gravity filling avoids. A crankshaft is typically mass-produced. This means the possible improvement in yield from pressurization could lead to larger cost savings.

An automatic digital pressure control system could be developed for the CFPS system. This would help to alleviate the CFPS misfires caused by increased pressure during the filling process, such as the one that occurred during the first trial

While the chilled inlet is effective at keeping the liquid metal in the mold after the vacuum is released, there is still the 30 second delay present. If a stopper valve could be developed to close the inlet immediately after the vacuum is released, waiting for the inlet to freeze would no longer be necessary. The valve would need to be able to withstand the extreme temperatures of liquid steel and be able to fall into the closed position much faster than the chilled inlet would solidify.

Currently *MAGMA*soft is not able to simulate the increased pressurization during solidification. It would be a valuable computational tool to be able to simulate various casting designs for the CFPS process without the need to physically test those designs first.

REFERENCES

1. Zoroufi, M. and A. Fatemi, "A Literature Review on Durability Evaluation of Crankshafts Including Comparisons of Competing Manufacturing Processes and Cost Analysis," in *26th Forging Industry Technical Conference*, 2005.

2. Williams, J. and A. Fatemi, *Fatigue Performance of Forged Steel and Ductile Cast Iron Crankshafts*, no. 2007-01-1001, SAE Technical Paper, 2007.

3. Melendez, A.J., K.D. Carlson, and C. Beckermann, "Modelling of Reoxidation Inclusion Formation in Steel Sand Casting," *International Journal of Cast Metals Research*, vol. 23, no. 5, pp. 278-288, 2010.

4. Campbell, J., "Stop Pouring, Start Casting," *International Journal of Metalcasting*, vol. 6, no. 3, pp. 7-18, 2012.

5. Campbell, J., "Chapter 2 - Entrainment," in *Complete Casting Handbook (Second Edition)*, pp. 17-90, Butterworth-Heinemann: Boston, 2015.

6. *Feeding & Risering Guidelines for Steel Castings*, in Steel Founders' Society of America, Barrington, Illinois, 2001.

7. Hardin, R., T. Hays, and C. Beckermann, "Pressurized Riser Casting Trials," in *Proceedings of the 55th SFSA Technical and Operating Conference*, 2001.

8. *Magma^5 Release Notes*, (version 5.2), MAGMA GmbH, Aachen, Germany, 2014

9. Sorensen, C.E., "Mold for Casting Internal Combustion Engine Crank Shafts," Ford Motor Co., *Patent US 1992677*, issued February 26, 1935

10. Chandley, G.D. and R.L. Sharkey, "Method of Casting Metal in Sand Mold Using Reduced Pressure," Hitchiner Manufacturing Co., Inc., *US 4340108* issued July 20, 1982

11. Chandley, C., et al., "Counter Gravity Casting Process for Making Thin Wall Steel Exhaust Manifolds," *SAE transactions*, vol. 106, no. 5, pp. 799-806, 1997.

12. Griffiths, W., et al., "Influence of Counter Gravity Mould Filling on the Reproducibility of Mechanical Properties of a Low Alloy Steel," *Materials science and technology*, vol. 23, no. 2, pp. 137-144, 2007.

13. Jazwinski, S.T. and S.L. Finch, "A New Method of Feeding Applied to Castings Made in Static Moulds," *Foundtry Trade Journal*, vol. 6, no., pp. 269, 1945.

14. Taylor, H.F., *The Pressure Feeding of Steel Castings at Pressures Higher Than Atmospheric Pressure*, in Final Report on SFSA Research Project No. 20, SFSA, 1948.

15. Desnizki, W.P., "Application of Risers with High Atmospheric Pressure," *IRON & STEEL*, vol., no., pp. 51, 1958.

16. Dong, A., et al., "Investigation of Thin-Walled In718 Castings by Counter-Gravity Investment Casting," in *Advances in the Science and Engineering of Casting Solidification: An MPMD Symposium Honoring Doru Michael Stefanescu*: Wiley Online Library.

17. *Astm E1417/E1417m16 Standard Practice for Liquid Penetrant Testing*, ASTM International, 2011.

18. Miettinen, J., "Calculation of Solidification-Related Thermophysical Properties for Steels," *Metallurgical and Materials Transactions B*, vol. 28, no. 2, pp. 281-297, 1997.

19. Schindelin, J., et al., "Fiji: An Open-Source Platform for Biological-Image Analysis," *Nature methods*, vol. 9, no. 7, pp. 676-682, 2012.